Chapter 3
Principles and Practice of Metallography

3.1 Sampling and Specimen Preparation

3.1.1 Sampling

One of the principal differences between metallography in modern material sciences or industrial quality control is that the taking of samples from objects of cultural heritage is usually a one-time procedure with very limited scope as regards sample size or position. When rare or valuable objects are permitted to be sampled for analysis, small samples can only be taken from inconspicuous locations. Therefore, there are a number of criteria that should be considered before any sampling is undertaken:

A. The microstructure of the samples should not be altered in the process of removal.
B. The sample should be representative of the object as a whole or of a selected feature or area of the object.
C. The orientation of the sample in its dimensional relationship to the object concerned should be marked on a photograph or a drawing of the object.
D. If it is not obvious from where the sample was taken, the position on the object concerned should be marked on a photograph or a drawing of the object.
E. The sample should be assigned a laboratory number together with sufficient documentation to enable its identity to be preserved.
F. The object should be photographed or drawn before the sample is taken. This is especially important if the dimensions of the object are fundamentally altered by the material removed.

Metallographic studies should be integrated as far as possible with archaeological data, such as date and geographical and cultural provenance. The chemical composition and technology of manufacture to extract the maximum benefit from the removal of a small sample from the object remains the most important. There are

D. A. Scott, R. Schwab, *Metallography in Archaeology and Art*, Cultural Heritage Science, https://doi.org/10.1007/978-3-030-11265-3_3

still far too many metallic artefacts lacking detailed provenance information because they were obtained from dealers, museum collections, private donors, etc., which lack documentation, or from uncontrolled excavations.

It is generally possible to undertake metallographic examination on whole objects without sampling, if a small area of the artefact can be polished, which is normally used on components that are too large for the laboratory and where sampling is not permissible (see Bramfitt and Lawrence [10]). Alternatively the whole object is mounted with a resolvable moulding material like acrylic resin and then ground and polished at the position of interest, analysed at this location and finally removed from the redissolved resin (see Blet-Lemarquand et al. [8]). This technique is especially useful for gold items, because of the high reflectivity of gold; the polished spots are invisible to the naked eye, and for small items like coins, which cannot be sectioned. However, the predominant methodology is to remove a small sample with the use of a jeweller's saw, or a scalpel, a vibro-tool cutter, hand-held micro-diamond wheel or a diamond cut-off machine, which is cooled ensuring that no microstructural alteration takes place during removal. Careful cutting with a fine jewellers saw is often the only choice in the field or in museum storage areas and care must be taken to avoid undue damage to the sample itself. For example, cutting away a tiny sample with a scalpel blade may create too much mechanical deformation, ruining the true microstructure of the object.

Figure 3.1 shows the deformation zone of a sample, which was taken by pliers. The advent of hand-held drills with small diamond wafering blades has made sampling much easier, as removal of a small sample with a jewellers saw from a hard material, such as medium-carbon steel, can take a considerable period of time by comparison. Very hard bronzes are also best cut using a miniature diamond tip in the field, while high-speed cut-off saws with diamond-impregnated blades are available in the laboratory.

Laboratory sampling of archaeological or art material has much in common with industrial practice if the object is large enough to be held in the diamond

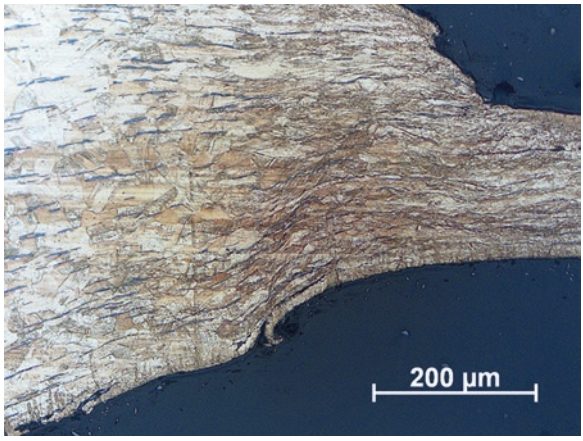

Fig. 3.1 Fragment from a Bronze Age shield (type "Nipperwiese") from Schiphorst, Schleswig-Holstein, Germany, which has been taken by pliers. Thickness reduction and slip lines are still visible at several hundred of micrometres away from the real cut surface (etched with acid ferric chloride)

blade cut-off saw, which is oil or water cooled, and with varying weights. Normal specimen holders offered by the manufactures are often not suitable for fragile, non-uniform and tiny samples from art and archaeology contexts. Pragmatism and creativity are therefore needed to convert commercial specimen holders or design suitable new ones. Speed of rotation and cutting weight exerted on the object can be varied to suit the material, producing a clean cut with no deformation or thermal damage to the sample whatever. A proper sectioning by a diamond blade cut-off saw offers a high-quality surface where a first grinding step with rough grinding paper can be omitted (see Aliya [1, pp. 233–35]; Geels [20, pp. 14–45]; Vander Voort [75, pp. 62–69]). If samples are big enough, an accurate cut into halves by a thin wafering blade and using the other part for other investigations can be a good strategy.

It might be surprising to some readers that we have to point out the following basic principle, but interdisciplinary working should be based on mutual understanding, though it is often connected with confusion in terms – especially when cultural scientists have to work together with different scientific disciplines. There is a fundamental difference between the microscopical examination of metals and biological or geological samples. This difference is due to the fact that all metals are opaque to optical light. This means that they do not allow light to pass through them, even the thinnest foils, although the greenish light which can be seen in thin gold foils is light transmitted through the grain boundaries. Therefore, metallic samples have to be prepared as polished sections and not as thin sections, and they are observed by reflected light rather than transmitted light.

3.1.2 Mounting

Specimens are usually too small to be handled in the preparation process and must be mounted in a suitable mounting material. Specimens were once mounted in molten sulphur, waxes, dental plasters, low-melting-point alloys and others (see Kehl [28]), so the reinvestigation of "old" samples sometimes produces some oddities and unpleasant surprises. These materials have caused much trouble, due to degradation, varying hardness, sensitivity to solvents, increased brittleness over time and difficulties in polishing and preparing a scratch-free surface and are nowadays replaced by polymeric materials such as epoxy, acrylic or phenolic resins (see Geels [20]). The criteria for the choice of a specific mounting material are dependent on the constitution of the sample and the scheduled analysis. Factors such as porosity, thermal sensitivity or hardness of the sampled material as well as the viscosity, the polymerization conditions and the hardness of the mounting material must be traded off (see Bousfield [9]; Geels [20]; Samuels [59]). Otherwise, mounting may negatively affect the preparation, damage the specimen or create trouble in subsequent examinations. The orientation of the sample in the mounting mould has to be carefully considered, and there is a danger that small fragments will float or otherwise be disturbed when resin is poured over them. To obviate these problems, the sample

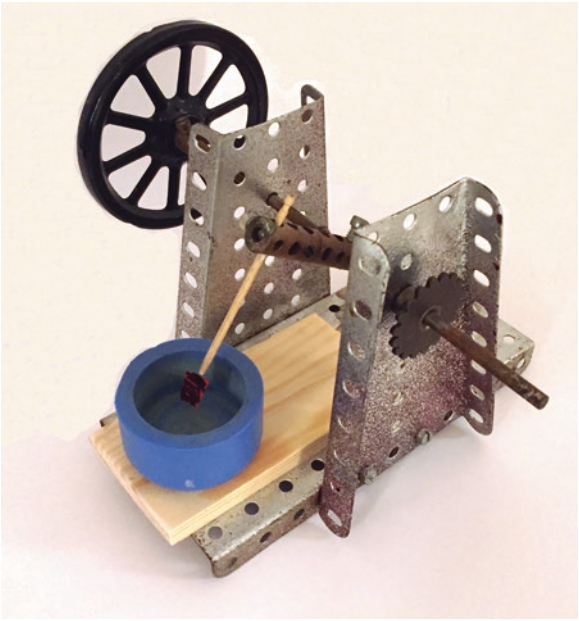

Fig. 3.2 Mounting jig for small samples attached on the end of a cocktail stick with adhesive

can be held in place on the bottom of the mould with a thin plastic strip, available from metallographic supply companies, or can be held on the end of a cocktail stick by a tiny blob of cellulose nitrate adhesive, with the stick held upright in a small clamp. Scott [67] has described devices of this type, and one of them is illustrated in Fig. 3.2. Dr. Shugar (personal communication) has used small silicon carbide discs mounted on wooden sticks, followed by small circles of felt with diamond polish for the preparation of small areas of large objects which cannot be cut and mounted, with some success. This obviates the need to cut and remove a sample from some types of artefacts which could be suitable for this approach.

If scanning electron microscope examination (SEM) or electron microprobe analysis (WDS-EPMA) is planned, where samples have to be electrically conductive, it can be useful to use a copper wire instead of the cocktail stick, and a conductive adhesive to fix the sample. Samuels [59] shows some helpful proposals for methods to make electrical contact with the back of a specimen mounted in non-conducting materials. Electrical conductivity is essential to scanning electron microscope examination or electron microprobe analysis (WDS-EPMA) to avoid electrostatic charging. Conductive mounting resins as well as fillers such as graphite, nickel or copper powders are commercially available. However, it should be pointed out that the high-count rate necessary for EPMA analysis requires specific mounting techniques and materials, because many polymers suffer deterioration under the impact of the electron beam. In addition, many mounting materials react with X-rays, used for X-ray diffraction or X-ray fluorescence analysis.

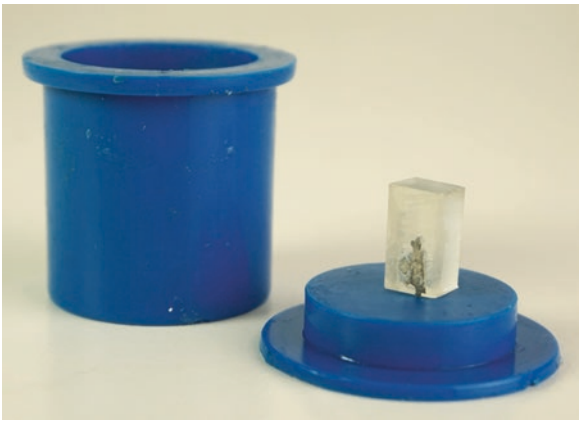

Fig. 3.3 Fragile tin sheet from a Roman tinned statuette from Trier, Germany, fixed on a small block of epoxy resin to stabilize sample position before embedding. (Photo by E. Duberow)

Many archaeological materials are heavily corroded and are therefore porous and mechanical unstable. The disadvantage of using the plastic or metal clip technique for archaeological material is that some of these materials are so fragile and corroded that they cannot be held in place because the force exerted by the plastic or metal may even be too much for the fragile sample, especially if it is an exceptionally thin piece of sheet. In this case, some small blocks of acryl glass or epoxy resin can be used to stabilize and to position the sample, as shown in Fig. 3.3. The samples can be fixed on the block with instant adhesive and then both embedded with resin. The porosity of those samples makes them difficult to prepare and to investigate. Their fragility and porosity causes pull-outs during polishing, and the cracks and pores can store air and humidity, which is troublesome for scanning electron microscope examination, as well as for light microscope examination, as alcohol, water or remaining acids can vaporize during the investigation. It is therefore profitable to infiltrate those samples, as well as ceramics or slag. Special low-viscosity resins are available from different providers, but impregnation is best done in vacuum.

Vacuum impregnation is the only satisfactory procedure and can be performed in homemade apparatus (Fig. 3.4) or if more regularly used, in equipment specially designed for metallographic purposes, shown in Fig. 3.5. The basic principle is the same, but commercially available apparatuses are more timesaving, as they allow the impregnation of several samples in one step. The samples must be placed in moulds, and then the moulds can be placed in a vacuum chamber. A vacuum pump has to pump out all the air from the pores, and then resin is sucked into the chamber, replacing the vacuum within the pores. After curing all voids should be covered and filled by the mounting material, and the specimens should be suitable for preparation and examination. The cups which are used for embedding the sample are made from silicon rubber or high-density polyethylene. Even with the use of a mould release agent on the surface of these embedding cups, they eventually degrade on contact with the epoxy mounting resin.

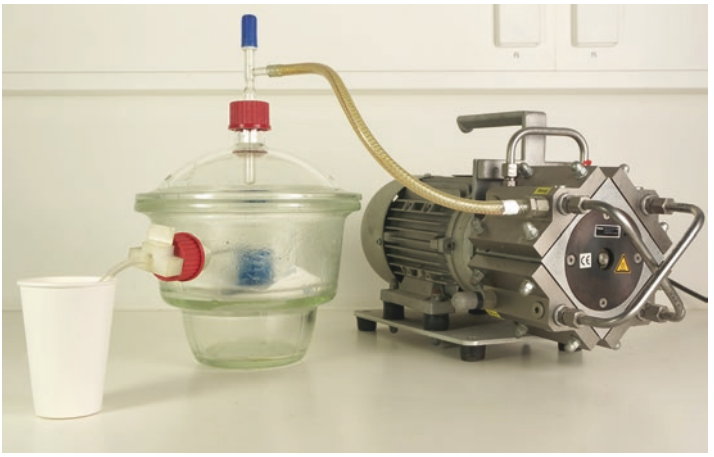

Fig. 3.4 Self-made apparatus for impregnation of single moulds, consisting of a desiccator, a vacuum pump and a tube to suck the resin in. (Photo by E. Duberow)

Fig. 3.5 Commercial vacuum impregnation system with a turntable, suitable for the impregnation of up to 14 moulds within one step and user-defined programmes for cycle time and levels of vacuum for different materials. (Photo by E. Duberow)

Silicon rubber cups are more readily degraded and eventually discolour and stick irreversibly to the epoxy resin used for the mounting. The resin itself is part of the problem, as these are subject to continual chemical remodification over the years, producing casting resins which have different mechanical and chemical properties. Regular use of a mould release agent will ensure that these moulds can be used for

many years. With the polyethylene cups, the authors have found that a thin smearing of butter or Vaseline around the inner surfaces of the mould is sufficient to avoid adhesion of the resin to the cup!

3.1.3 Grinding and Polishing

The preparation methods have changed over time, and some practices have been abandoned, and others have been modified. Grinding and polishing are elemental steps in the metallographic specimen procedure, even though the techniques applied have altered significantly. Advances have been made in terms of polishing compounds, and there are now available a number of different polishing materials for the modern metallographer.

Commercial providers for material preparation have designed consumables and especially equipment for fully automated grinding and polishing, electrolytic and vibratory polishing, which are usually not standard in archaeometric laboratories. Apart from that, electrolytic polishing of archaeological materials should be avoided, because electropolishing does not only completely remove all traces of mechanical grinding and polishing operations but also all non-metallic compounds, as Fig. 3.6 illustrates, which would have provided valuable information.

We refer to more or less traditional standard preparation practices which have wide applicability and which can be modified according to the requirements of the

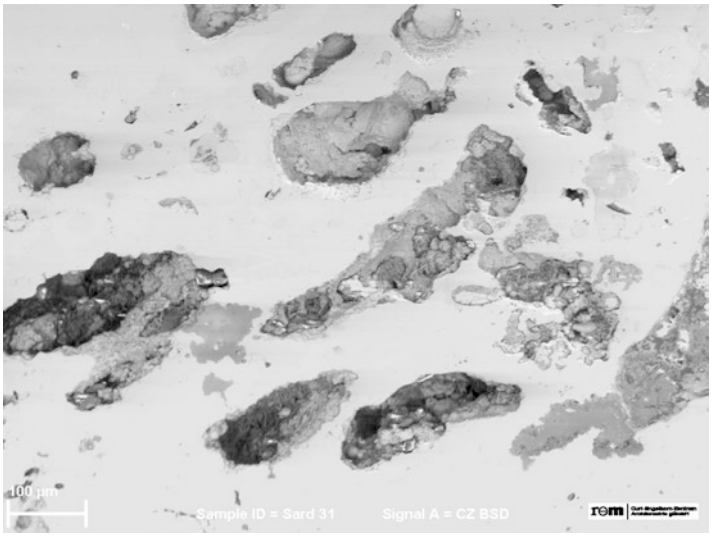

Fig. 3.6 SEM image of the surface of an oxhide ingot from Sardinia (original sampled by U. Zwicker). The sample has once been electro polished for EMPA, which removed all non-metallic components and left deep craters

materials. The standard literature provides many examples for automated or manual preparation procedures for nearly every specific material and can be consulted for further information [20, 34, pp. 61–142; 46, 59, 75, pp. 127–266; 76]. Although care has to be taken in applying standard industrial metallographic practice to ancient metals, as often several minutes of grinding of samples are recommended for industrial alloys, which would be impractical for ancient specimens, whose size frequently precludes such thorough preparation techniques, there would simply be no sample left to study! The smaller the sample is, the greater the degree of care which has to be exercised in its preparation.

The mounted sample is ground on wet silicon carbide papers or diamond grinding discs. Abrasive material is also available as powders in suspensions. Grinding hard materials requires a different type of surface than grinding softer materials; also, the size of the sample and the roughness of the surface influence the choice of grinding material and grit size. Grinding must remove surface damage and eliminate every roughness, using progressively finer abrasive grits. Plane grinding by coarse grit size paper is the first step in the grinding process to ensure a uniform plane surface. Coarser grit size papers (<P 240) are usually not necessary for ancient metals. Such papers are often used in belt grinders, which have widely been used in metallographic laboratories to produce a flat surface of the specimen before embedding [28, pp. 3–4 ; 75, p. 98], but these are best avoided for most ancient and archaeological samples as there is a danger of too much surface damage to the material. The succeeding paper should be one or two grit sizes smaller than that used before and employed to erase all previous grinding scratches. The grit size numbering systems of silicon carbide papers are stated according to the American ANSI standard (American National Standards Institute) or the European FEPA standard (Federation of European Producers of Abrasives), which differs as to how they designate the size of the silicon carbide grit. For example, the FEPA paper grit number P1200 has nearly the same grain size (≈ 15 μm) as ANSI grit number 600 (see Vander Voort [76, p. 1093]). These different standards must be kept in mind by the following recommendations for preparation from the literature. The final grinding step should finish with the finest grit size that is necessary to leave a flat and uniform surface. All grinding should be done wet to wash away all grinding debris and to keep the specimen cool. Specimens should be cleaned after each grinding step to remove grinding debris to avoid contamination during the next preparation step. A jet of water, compressed air and especially a final cleaning in an ultrasonic bath are effective cleaning methods [59, p. 260; 75, p. 72]. Wiping clean with cotton wool under flowing water can only be done for harder materials, whereas silver, gold or unalloyed copper can easily be scratched by natural cotton wool (see below). Washing in ethanol or methanol from a wash bottle followed by drying is recommended.

Polishing on synthetic napped cloth wheels using diamond powder suspension in water as the polishing agents with a compatible lubricant is the final step in producing scratch-free surfaces. Diamond suspensions are usually 6 micron diamond to 1 micron diamond. If required, a finer finish can be obtained using colloidal silica or 0.25-micron diamond in water or oil suspension, but for many purposes, polishing down to 1 micron is sufficient. Silicon oxide suspensions have been well proven

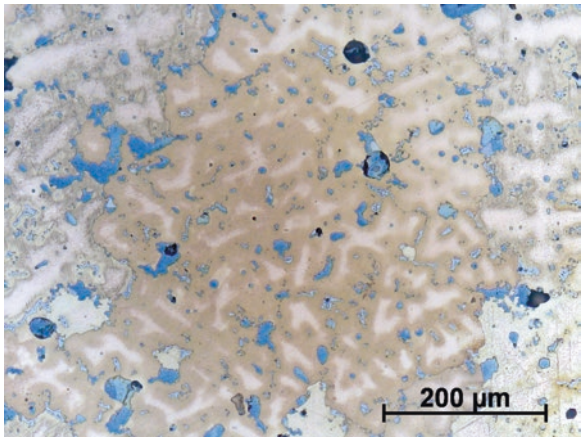

Fig. 3.7 Casting waste from the Late Iron Age oppidum of Manching, Germany, with 7.2% Pb and 9.5% Sn. Micro segregation is revealed, and lead inclusions have lost the typical black smearing and turned to blue-grey after a final attack polish step with aluminium oxide and ammonium hydroxide

over the years in producing almost perfectly polished surfaces. Colloidal silica is useful for the removal of scratches from the diamond stage of polishing if they cannot be otherwise eradicated but can also form a film on the polished surface of the sample, which must be removed with water. As colloidal silica has a tendency to coagulate, the supernatant liquid should always be used for final polishing. Aluminium oxide or other abrasives (see Petzow [46], table 1.5) have become less important and have been widely replaced by diamond suspensions, because of its universal application and the high removal rates. Indeed in certain cases, an aluminium oxide polishing on a suitable cloth such as matted wool with or without a little neutral liquid soap can achieve excellent results, shown in Fig. 3.7 as soft metals like tin or lead are not effectively polished with diamonds.

Particularly scratch-free surfaces of soft materials such as copper or silver alloys can be achieved by so-called attack or etch polishing, when chemical polishing is combined with mechanical polishing by the addition of a dilute etchant to the abrasive. The combination of chemical activity and mechanical abrasion produces scratch-free and deformation-free specimens, although the process is hard to control due to the great variation in properties and composition of ancient and historic metals. Some sellers provide alkaline, with a pH of about 10, or acidic, colloidal oxide suspensions, which are ready to use or are suitable for mixing with chemical reagents for attack polishing. Some attack polishing additives are listed in the literature [20, 59, tab. 9.1; 75, pp. 543–551; 76, pp. 1107–1110]. By reducing the dilution of the etchant and an extension of the polishing time, a small but noticeable relief between the grains can be achieved, which can be useful for special microscopy techniques such as differential interference contrast (DIC), orientation contrast in the SEM or colour etching.

All grinding and polishing can be done manually by hand, or using automated grinding and polishing equipment, but many samples from cultural heritage are so tiny that only careful manual preparation is possible. In any case, the correct amount of pressure applied must be determined by experience since some materials quickly

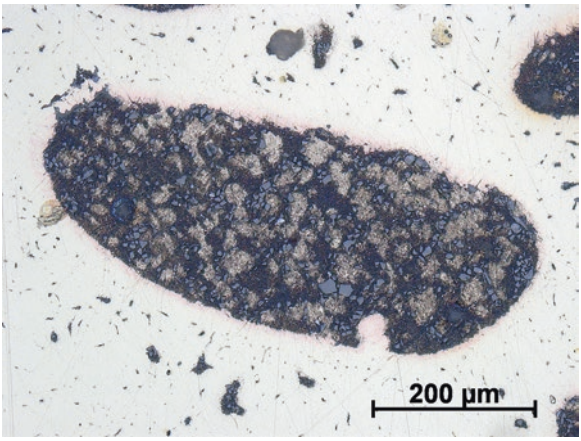

Fig. 3.8 High-leaded bronze belt ring from the Late Iron Age oppidum from the Martberg (Germany), with embedded abrasive fragments in the lead globules, because of too high polishing force

become deformed and annealed, producing false structures, or abrasives get easily embedded on the surface, as shown in Fig. 3.8.

Especially soft metals such as lead and tin are difficult to prepare, and papers should be waxed with paraffin to prevent embedding of particles. They are also prone to the introduction of false structure due to high polishing pressures producing a pseudo structure by twining and spontaneous recrystallization. Scott [65] has published an etch-polish technique for ancient lead which gave good results. Hard phases like intermetallics can crack, especially by automated polishing with too high pressure. On the other hand, if the pressure is too low, scratches will retain until the end of the final polishing step.

The quality of the preparation can significantly influence the response of the sample to the etching process. Specimens to be colour etched or examined with polarized light require a high-quality surface and should be polished with particular care, while techniques like EBSD are extremely sensitive to surface disturbance and need special procedures for preparation. After final polishing, the specimen surface must be cleaned carefully with alcohol and sufficiently dried before any investigation. Care must be taken at this stage to avoid drying marks on the surface of the sample. This may require careful attention with archaeological materials to avoid difficulties in the etching or visual examination of the specimen surface.

3.1.4 Etching

When mounted samples are studied, the surface of the metallic specimen should be examined first in the freshly polished state (see Sect. 3.2), followed by etching with a suitable chemical solution. Very important samples where the interface between the corrosion crust and the metal may be reserved for examination in the polished condition only, as etching may attack and remove the corrosion crust and non-metallic inclusions. Etching reveals metallic structure, but the importance of the

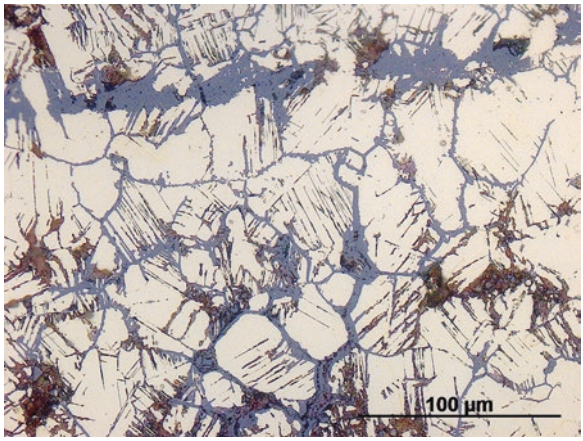

Fig. 3.9 Microstructure of a brass jug with 17% zinc and 1.4% lead from Khorasan region in Central Asia, dated to the second half of the twelfth century AD. Slip planes and grain boundaries are outlined by selective corrosion during burial

corrosion interface may be paramount, especially in authenticity studies, frequently required in the case of ancient bronze and silver artefacts. Microstructural features may be selectively etched or pseudomorphically preserved on metallic surfaces, which allows this technique to reveal micromorphology directly, as Fig. 3.9 illustrates.

A list of suitable etchants is given in the Appendix. A very comprehensive list of different etchants for all purposes is given by G.F. Vander Voort [75], whereas most conventional etchants and their applications are described in all the standard literature (see, e.g. Geels [20]; Lyman [34]; Petzow [46]; Vander Voort [76]). A useful online source of scores of different etchants is that provided by the Etchant's Database (http://www.steeldata.info/etch/html/overview.htm).

Etching must reveal microstructural characteristics, which are not yet evident in the as-polished condition and must produce contrast between the features of interest and the other microstructural components. Contrasting only by optical techniques will be reviewed in Sect. 3.2. Etching is a controlled selective corrosive attack, affecting preferentially a specific phase, by using a chemical solution, which is called the etchant. An etchant is a combination of either an acid or base with an oxidizing or reducing agent in a solute such as water or alcohol, but also glycerine or glycol or other media can be used. Aqueous solutions usually etch more rapidly than alcoholic solutions. By chemical etching, a surface relief is produced by local redox reactions, whose actual process and extent are based on the different local electrochemical potential of the microstructural constituents [46, pp. 40–43]. The local dissolution of some microstructural features changes the reflectivity of the surface by roughening or even staining it by the deposition of a thin surface film. The incident light then is reflected, diffracts or gets absorbed, or topography gives grey scale values by shadowing, producing an optical contrast. Colour contrast can best be achieved by the interference layer technique, which is based on coating the surface with interference layers by evaporation, sputtering or chemical deposition (see Bühler and Hougardy [12]). The latter is called immersion colour etching or tint etching, which can be performed without the need for additional technical

equipment (see Vander Voort [77]). Many of these colour etchants, also used extensively in this volume, were originally devised by Klemm [29, 30], Beraha [5, 6]; Beraha and Shpigler [7] and Vilella and Kindle [80]. Frequently, copper alloys etch rather quickly, especially in alcoholic ferric chloride, and dilution of some etchants with additions of alcohol may be necessary to prevent too rapid etching.

Contrast enhancement by etching is due to inhomogeneity within microstructures, and therefore the rates of surface-etchant interaction vary locally and temporally. Differences in phase compositions, but also large differences in lattice orientation and crystal imperfections, are contrasting features revealed by etching. Composition and physical condition of the specimen are factors that influence the time of etching. Two-phased or multiphased alloys generally etch more rapidly than single-phased alloys, because of the local difference in electrochemical potential of the phases, forming a corrosion cell with anodic and cathodic regions [46, pp. 40–43].

Displacements by cold working in certain regions are also readily attacked and produce a high contrast because of the differences in orientation of the reflected light, shown in Fig. 3.10, but also grain boundaries are nothing else than lattice defects and retain internal energy. This is why grain boundaries have a higher dissolution potential than the grains themselves and some etchants – usually strong oxidizing agents – reveal grain boundaries, whereas other etchants produce more uniform surfaces and reveal the different crystallographic orientation of grains, which are randomly sectioned in the polishing plane of the sample.

It should be noted that etching reagents can be used to produce very particular effects, which can introduce errors in the interpretation of microstructure, due to selective attack that some etchants may cause. Oberhoffer's reagent, for example, which is used to reveal segregation in ferrous metals, deposits copper from the solution on the phosphorous-rich regions of the sample and prevents any further attack to these parts, while segregation-free regions are deeply etched without bringing out the structure fully. Reagents which are based on sodium thiosulphate or potassium metabisulphite solutions such as Klemm's or Beraha's reagents form sulphide films on metal surfaces which show affinity to sulphur but only slightly affect regions

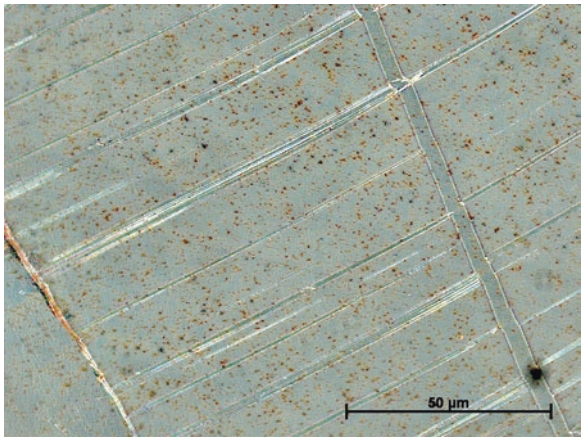

Fig. 3.10 Slip lines in gilded silver phalera from Uročišče Kruglik, Ukraine, dated to the end of the second century BC. The parallel steps on the surface become visible after etching with acidified potassium dichromate viewed with polarized light

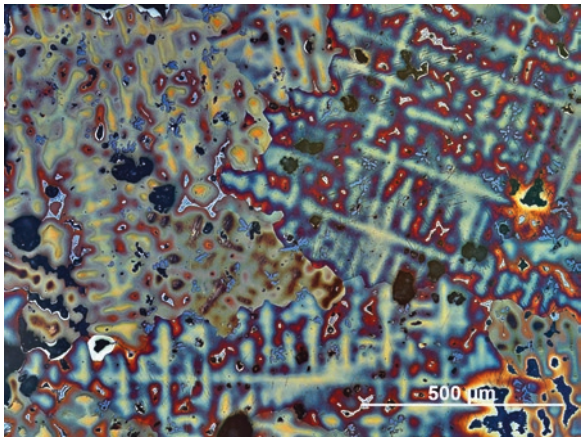

Fig. 3.11 Coarse crystallites of solid solution in the bronze part of a bracelet from the Royal tomb of Lori Berd, Armenia, containing dendritic micro segregations. Interdendritic tin segregation and $\alpha + \delta$ between primary α_{Cu}-solid solution is clearly revealed by etching with Klemm's reagent III

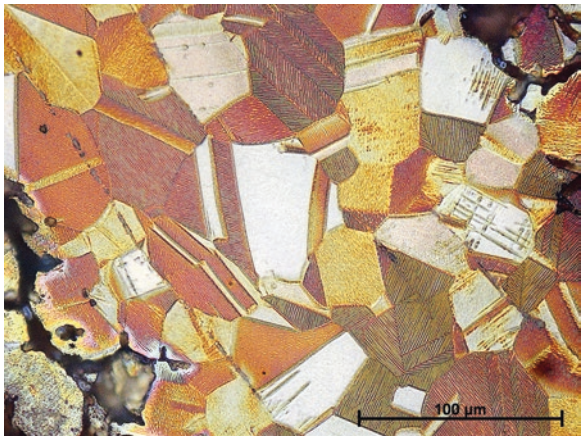

Fig. 3.12 Recrystallized α-brass of a gladiator helmet from Herculaneum (see also Figs. 3.21 and 5.17). Klemm's reagent II has produced pattern of parallel lines on the individual twins and grains which are related to their crystallographic orientations

with elements with low affinity to sulphur. For this reason, these etchants are very sensitive to the concentration gradients caused by segregation of alloying elements, as shown in Fig. 3.11, but also to crystallographic texture, revealing preferred orientations as can be seen in Fig. 3.12.

Indeed many standard etchants have been developed to evaluate the overall structure, but as this general requirement is not always achieved satisfactorily, double or multiple etching are sometimes employed, by using different etchants sequentially – mostly grain contrast etchants combined with grain boundary etchants. Colour etching procedures sometimes recommend attack polishing, some slight relief polishing or pre-etching with standard general-purpose etchants to achieve good results (see Beraha and Shpigler [7]; Vander Voort [77]). Increasingly, the authors have become aware of the advantages of colour etching in the preparation of archaeological material [68]. The reasons for this are, firstly, that grains can be delineated without deeply etching the sample, as in conventional etching, and that corrosion crusts are not necessarily disrupted by this technique. Secondly, the presence of casting segre-

gation is very sensitive to colour etching, and since many alloys retain some aspect of this, it is clearly visible in the etched sections. Care should, however, be taken to repolish the sample before long-term storage as corrosion may still occur in storage. Some samples with incipient bronze disease must be stored at relative humidity's less than 30%; otherwise, continued slow corrosion of them will occur. With fragile ironwork suffering from akaganeite corrosion, storage at less than 19% relative humidity may be necessary.

Most conventional etchants work by immersing the specimen in a suitable reagent, while others will not work without swabbing a cotton wool swab saturated with the reagent over the surface. At this point, it might be helpful to proffer some advice that there is a danger of scratching soft metals such as unalloyed copper, gold or silver, by swabbing with natural cotton, and therefore semi-synthetic viscose wool should be used instead. Some etchants have to be heated or even boiled, but most etching can be performed at room temperature. Heavily strained bronze sheet may etch in alcoholic ferric chloride, one of the standard etchants at a very fast rate, so some experience has to be gained in the length of time; a sample is submerged in an etching solution. The best course is often to immerse for a few seconds only and then gauge the result. If further etching is required, the sample can then be reimmersed for a further few seconds. Dilution of some of the standard etchants may be advisable in certain cases. Some colour etching processes take many minutes rather than seconds, and this has to be gauged carefully by the investigator depending on the alloying system involved.

A final instruction must be given concerning safety precautions, especially with the handling and storing of etchants. Most etchants are dilute chemicals with one or more active ingredients in a solute, and many etchants can be quite safely handled for specimen preparation. Indeed the single ingredients can already be dangerous, as highly concentrated acids or bases are needed to mix the reagents. Some ingredients are hazardous to the health, some are toxic, some are flammable, and some are strong oxidizing agents, while others are reducing, and mixing them together can result in violent or even explosive reactions. It is therefore essential to consult the Material Safety Data Sheets of the ingredients and the literature (e.g. Geels [20]; Petzow [46]; Vander Voort [76]). Some etchants like Beraha's colour etchants form hydrofluoric acid (HF) when ammonium difluoride (NH_4HF_2) dissolves and must be used and stored in plastic containers. Used etchants should not be disposed of except in specialized containers for safe disposal of laboratory waste.

3.2 Light and Electron Microscopy

3.2.1 Light Optical Microscopy (LOM)

Having created a flat and highly reflective surface, examination of the section can utilize the optical light microscope, preferably a metallograph, and samples can also be placed in the electron microprobe (EPMA), in the scanning electron microscope

(SEM), or analysed with X-rays such as X-ray fluorescence (XRF) or X-ray diffraction (XRD) techniques, all of which are invaluable in a comprehensive study of metallographic sections. All chemical and structural analysis should be done before etching the surface. Electron beam or X-ray analysis is non-destructive, and the specimens are kept ready for microstructural analysis, whereas all laser ablation (LA-ICP-MS or LA-ICP-OES) and especially glow discharge techniques (GDOES or GDMS) leave veritable craters on the surface and the specimen must be prepared again. Therefore, the first and basic procedure is to start with optical light microscopy (LOM) using incident bright-field illumination to get an overview of the section. For reflected light microscopy, the light passes directly onto the specimen surface and reflects back through the objectives to the eyepiece. By the absorption of some wavelengths of the incident white light, their complementary colours are reflected back, for which reason metals such as copper or gold appear coloured, whereas most metallic phases have a very high reflectivity over the entire range of the visible light and cannot be distinguished from each other. Therefore, phase contrast of opaque materials is very poor under bright-field illumination, but topographical features that are at an angle to the incident light reflect the light outside the objective lens and appear dark. Most metallic microstructural constituents show reflection differences which are too low in contrast and are not yet evident in the as-polished condition viewed in bright field, but pores and cracks, non-metallic inclusions, corrosion products and also many intermetallic compounds are already detectable by their lesser or greater reflectivity. They can be documented and quantified only by distinguishing them by their general optical characteristics, with no general necessity of exact identification (see Sect. 3.3.2). To enhance the optical contrast to reveal further microstructural details, the reflection capacity of the surface of the specimen must be increased by etching or by changing the illumination mode. Dark-field illumination or polarized light is an optical method to enhance the contrast without any alteration of the surface and should be used for further evaluation of microstructure [68]. The contrast produced by dark-field illumination is negative to that viewed in bright field as dark fractions appear bright and vice versa. Its application is useful for the identification of some non-metallic inclusions and for improving contrast to surface irregularities. Much more revealing than dark field is the use of polarized light, as many non-metallic compounds such as inclusions or corrosion products, but also some metals and alloys, are optical anisotropic. Most crystals except the cubic system are optical anisotropic and show double refraction of the polarized light from the surface. This birefringence produces manifold local colour effects without the need for additional etching, which can be intensified by tint etchants (Fig. 3.13). Crystals with a cubic symmetry or amorphous materials are normally optical isotropic, which means that their optical properties are the same and do not change the state of polarization by reflecting the light uniformly in all directions.

Optical isotropic materials do not respond to polarized light and remain dark. Anisotropy of non-metallic inclusions and isotropy of most metals have predestined polarized light microscopy for the identification of non-metallic inclusions in metals and alloys.

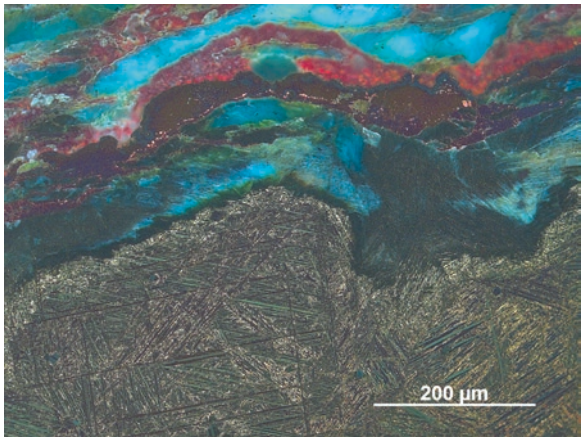

Fig. 3.13 Corrosion layer and microstructure of a high-tin (29% Sn) bracelet from Southeast Asia. The acicular β-phase needles are best viewed under bright-field illumination after tint etched with Klemm's reagent III, but viewed with polarized light, the β-phase is still observable and the alternate bands of the corrosion layers are revealed

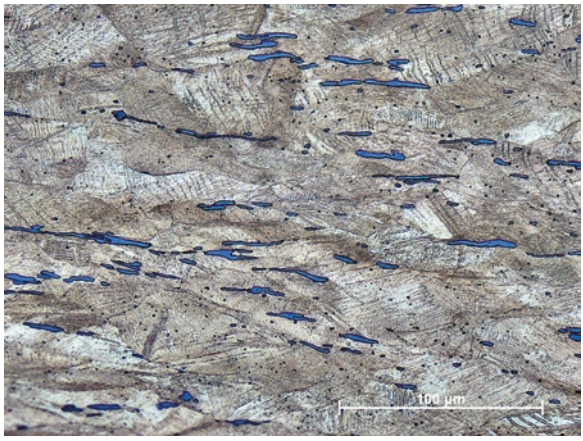

Fig. 3.14 Elongated copper sulphide inclusions within a cold-worked metal matrix of an Urnfield bronze cup appear blue-grey under bright-field illumination. Their mean volume fraction has been determined by area analysis A_A to be 1.5%

The best known application for ancient and modern alloys is to distinguish between cuprous oxide and copper sulphide inclusions, which both appear bluish-grey under bright-field illumination (Fig. 3.14). These two minerals can already be distinguished in the bright field with some experience, but they can be clearly differentiated by viewing in dark field or in polarized light (Fig. 3.15). Cuprite (Cu_2O) has a cubic structure and should appear dark, but it shows a strong anomalous anisotropy effect and gleams bright ruby red under dark-field illumination or polarized light, shown in Fig. 3.16.

The colour variation can be from yellow-red to pale reddish. Authenticity studies tend to take the axiomatic view that bright red crystalline cuprite is a good indication of the authenticity of the bronze or copper alloy concerned and is a distinction with a long pedigree and a general consensus. Cuprite is also one of the most common corrosion products of ancient copper alloys, which immediately overlays the original metallic surface [66]. Scott [64] and Piccardo and co-workers [48] have shown the colour change of cuprite from ruby red to orange and finally to yellow to

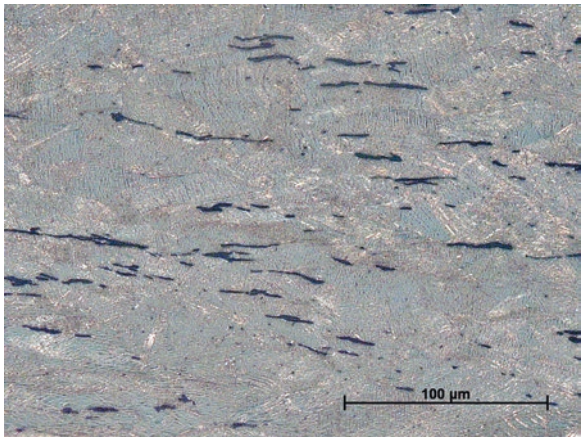

Fig. 3.15 Same as Fig. 3.14 viewed under polarized light. Copper sulphide inclusions and metal matrix are optically isotropic and appear dark

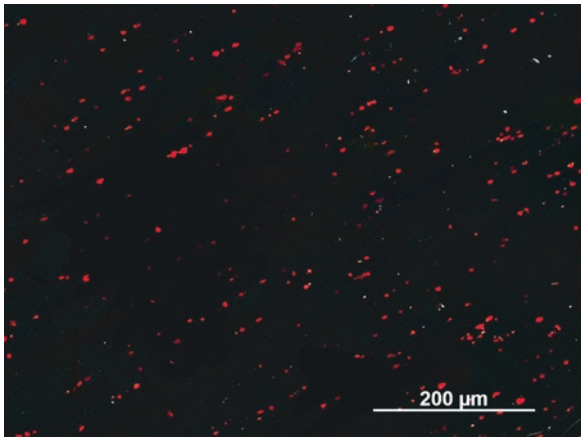

Fig. 3.16 Copper oxide inclusions in the Eneolithic copper disc from Hornstaad viewed under polarized light. Their volume fraction V_V has been determined by area analysis A_A to be 0.29% in total

be influenced by the increased presence of tin oxides in the corrosion layers of bronze, and an example is shown in Fig. 3.17.

A similar effect can be observed for brasses. Multiphase corrosion layers containing miscellaneous anisotropic phases may be differentiated and identified under polarized light, but also grain or dendritic structure and twins of some metals and alloys are revealed by polarized light due to their different crystallographic orientations. Ancient and historic metals which are known to be active to polarized light are antimony, arsenic, tin or zinc, but also some of their alloys [45], Tab. III). Figure 3.18 shows the grain structure of an Early Bronze Age tin bead from Southern Germany, revealed by polarized light.

Copper is an isotropic metal and inactive to polarized light, but arsenic is anisotropic, and von Schwarz [81] found anisotropy in high arsenical copper alloys. Figure 3.19 shows the microstructure a hypereutectic arsenical bronze viewed under polarized light. The position of this image is identical to Fig. 5.9, which has been recorded in

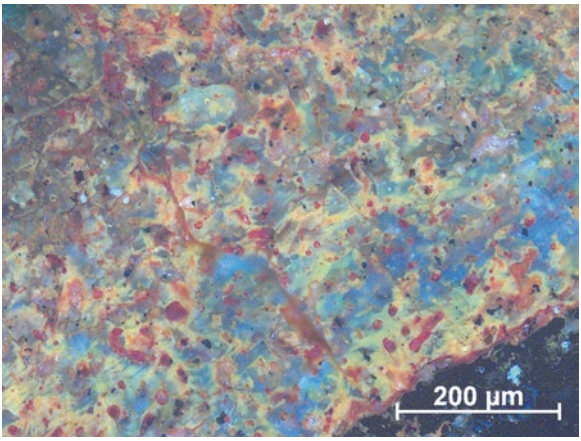

Fig. 3.17 Corroded surface of a life-sized Greek statue, so-called Agon, from a shipwreck found near Mahdia, Tunisia, viewed under polarized light. The alloy is tin-rich and the mineralized surface contains mainly of tin (hydro-) oxides with some relicts of cuprite

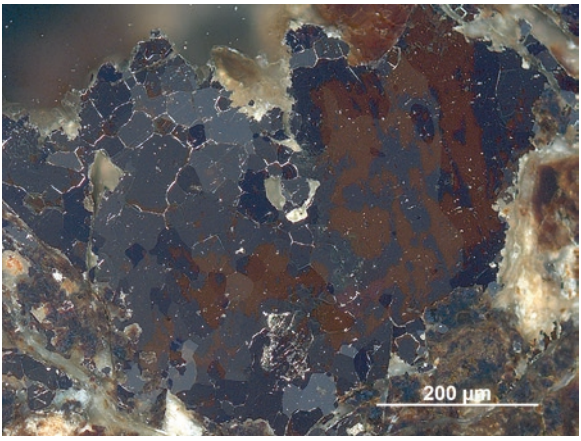

Fig. 3.18 Badly corroded Bronze Age tin-bead viewed under polarized light reveals grain structure of the metallic parts without etching

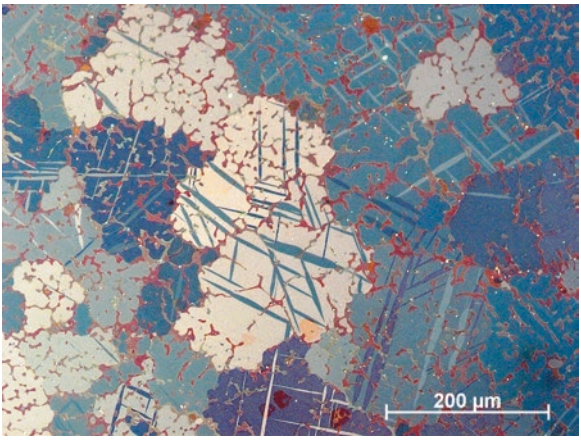

Fig. 3.19 Cross section of the arsenic rich part of the bracelet from Lori Berd, Armenia, viewed under polarized light, revealing coarse-grained aggregates of twinned α_{Cu}-Cu_3As eutectic

bright-field illumination, showing a dendritic as-cast microstructure. Viewed under polarized light, the equiaxed grains with twin bands appear, and EBSD measurement has revealed that it has a pseudo-hexagonal structure, corresponding to the mineral Domeykite, which is identical to the intermetallic γ-phase ($Cu_{3-x}As$) of the Cu-As equilibrium diagram (Fig. 5.7). Cubic α-Domeykite, shown in Fig. 4.18, does not respond to polarized light. Isotropic metals that are inactive to polarized light must be treated to create an optical effect by adequate etching procedures (Sect. 3.1.4).

3.2.2 Scanning Electron Microscopy (SEM)

Here we refer exclusively to scanning electron microscopy (SEM), as other electron microscope techniques such as transmission electron microscopy (TEM) need special specimen preparation, whereas specimens ready for light optical microscopical examination can directly be studied with high-resolution imaging and microstructural and microchemical analysis in the SEM. In the latter case, the specimen must be electronically conductive (Sect. 3.1.2) but can be examined in an etched or unetched condition, although usually the unetched state is preferred.

SEM and electron microprobe analysis have become common tools in material sciences as well as in the study of nearly all ancient materials over many decades (see Olsen [43]; Meeks et al. [36]). Cameca (Compagnie des Applications Mécaniques et Electroniques au Cinéma et à l'Atomistique) launched the first commercial electron probe microanalyser (EPMA) in 1958 [52, p. 2], and the Research Laboratory for Archaeology and the History of Art in Oxford has been engaged in the development of a microanalyser for archaeological applications nearly simultaneously [54]. The first commercial scanning electron microscope was produced by Cambridge Scientific Instruments in 1965 [52, p. 2], and a secondary electron image of an ancient granulation work appeared already in the same year [41, p. 226]. Schaaber [60] demonstrated practical application of the microprobe to metallography of ancient metals by analysing slag inclusions in Celtic and Roman iron finds, while Panseri and Leoni [44] examined nickel-cobalt segregation bands in an Etruscan spearhead. It is possible that Darling and Healy [13] published one of the earliest backscattered electron images of the microstructure of a Greek coin. Today many metallographic examinations of archaeological metals are totally based on SEM examination without any support of optical microscopy. Indeed, the SEM is one of the most versatile instruments for investigating ancient metals, but in our opinion, SEM cannot be regarded as a complete substitute for LOM. SEM offers several major advantages over the optical microscope such as much higher resolution, higher magnification, better depth of field and most of all its chemical- and structural analysis ability, but it provides no real colour differentiation, and many contrasts are more distinctly viewed with optical light. A skilled metallographer can identify and outline the phases and their distribution quickly and comparatively easy by the application of LOM. Another, but less objective reason is the aesthetics of well-prepared and proper etched microstructure viewed under an optical micro-

scope. An Instagram site by one of the author (Scott) called *Davidscottmetals* is a good illustration of the aesthetic approach to metallographic imagery.

There are numerous excellent standard textbooks devoted to principles of scanning electron microscopy and microanalysis, which should be consulted for further information and the deep knowledge they possess (see, e.g. Goldstein et al. [22]; Heinrich [25]; Reed [52]; Reimer [53]), but it is essential to the application of SEM in metallography to briefly introduce its basic function and mode of operation.

In the SEM a finely focused electron beam scans across the surface of the specimen and forms a two-dimensional raster of various signals point-by-point. These signals are based on the interaction of the beam with the target material, producing imaging signals and X-rays, which must be collected by an appropriate detector. For most conventional metallographic applications, the microscope column and the chamber must operate under vacuum conditions (10^{-3}–10^{-5} Pa) to avoid scattering of the accelerated electrons by gas molecules. Lang [32] showed that it can be useful to work at low vacuum (50 Pa) without conductive carbon coating to analyse carbon-nitride precipitations in Early Iron Age falcatae. These instruments operate with retained vacuum in the column, but with low vacuum in the chamber. The operator can vary the pressure – 10 Pa to 2700 Pa are possible in modern instruments – or must reduce the accelerating voltage to balance the charge of non-conductive substances for investigation without coating or other preparation techniques (see Goldstein et al. [22]; Stokes [71]). General terms for such an instrument are variable pressure SEM (VP-SEM), extended pressure SEM (EP-SEM) or environmental SEM (ESEM), but there also some other acronyms such as natural or atmospheric SEM (ASEM), which the latter is a little bit misleading, considering that average atmospheric pressure is more than 100,000 Pa. Working with low vacuum means that gas is present in the chamber and the beam electrons interact with gas and form a so-called skirt of scattered electrons. The skirt radius depends on working distance, pressure, beam energy and property of the gas (see Goldstein et al. [22]; Stokes [71]). For practical application of X-ray microanalysis in the VP mode, it should be clear that with increasing skirt radius, X-rays may be generated hundreds of microns away from the impact point of the beam and elements begin to appear in the spectrum which shouldn't be there according to the corresponding SE/BSE image (see Goldstein et al. [22]; Stokes [71]).

Again, in conventional metallographic work with the SEM, the sample must be conductive because the irradiated specimen is negatively charged by the beam. It must be vacuum resistant and stable against electron bombardment. In an electron microscope, an electron gun (thermionic W or LaB_6, or field emission cathode) emits a beam of electrons, which is accelerated towards the specimen and focused by electromagnetic lenses. The electrons of the beam collide with the atoms present in the sample so that the speed and direction of the incident electrons change; they are scattered both elastically and inelastically. Inelastic scattering means that the incident electrons lose energy during the penetration of the specimen surface. This energy may be transferred to electrons of the specimen atoms, generating an image and an analytical signal, or emitted as continuous X-rays, the so-called Bremsstrahlung, which is the main background of every primary X-ray emission

spectrum with energies from nearly zero to the maximum energy of the electron beam. If the transferred energy is high enough for a loosely bound valence electron to escape from the atomic shell and the kinetics are still high enough to get through the solid and leave the surface, it can be gathered by a positive biased collector as so-called secondary electrons (SE). Their exit energy is very low, and therefore only those that are generated at shallow depths of the order of a few nanometres are released from the surface. The intensity of secondary electrons is therefore dependent on the surface topography, where protruding positions emit more electrons than fissures and holes, where most electrons lose all of their energy and are reabsorbed. Secondary electron mode can be compared to the incident bright-field illumination in the LOM, as topographical features can be viewed with a very large depth of focus, whereas flat specimen in the as-polished condition do not show much contrast. SE mode is useful in examining the surfaces of objects, as shown in Fig. 3.20, fracture surfaces as shown in Fig. 3.21 and etched specimens, illustrated in Fig. 3.22.

The analytical signal is due to inelastic scattering by more tightly bound inner shell electrons, having the greatest binding energy, which requires higher energies to remove them from their orbitals and which is a less frequent event. When an electron in an inner atomic shell is ejected by an incident electron, leaving the atom ionized with an electron vacancy in its inner shell, it gets replaced by the transition of an orbital electron from a higher energy level. During this internal rearrangement, X-rays are produced, as the energy difference between the two levels is emitted. Therefore, each transition of electrons is characteristic for a certain energy level within the atomic union and the energy emitted as X-rays is characteristic for a

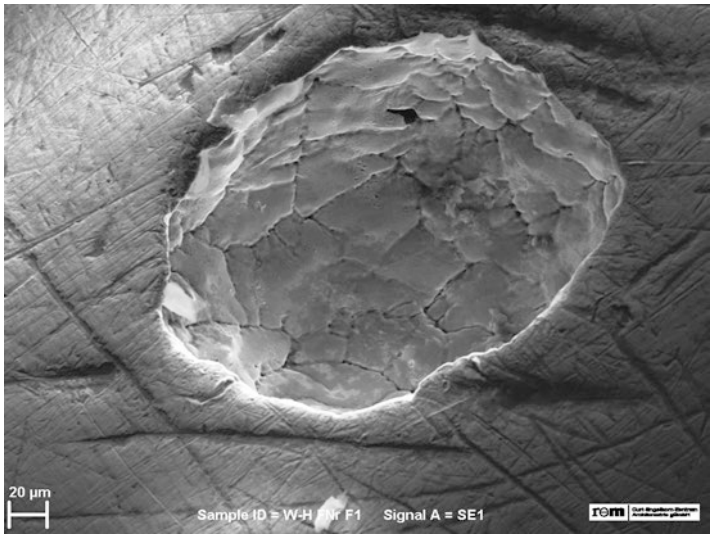

Fig. 3.20 Secondary electron image of the surface of an Early Iron Age gold ring from Worms-Herrnsheim burial showing deep blowholes

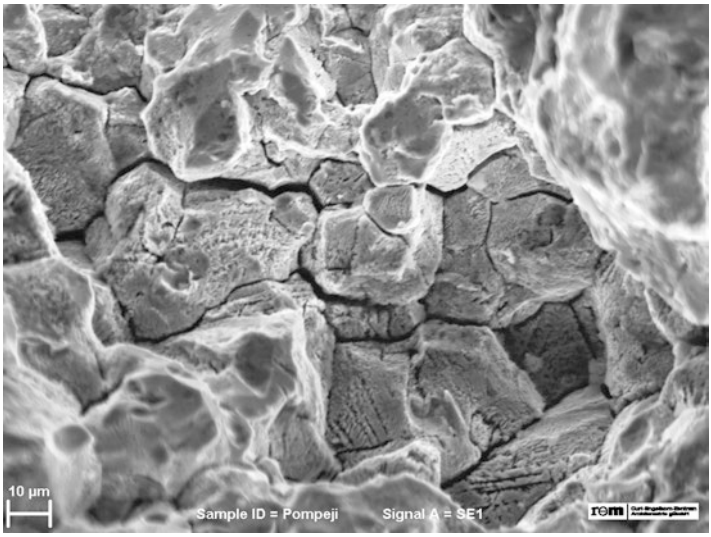

Fig. 3.21 Stress corrosion cracked brass alloy of a Roman gladiator helmet from Herculaneum, Italy (first century AD). Intergranular corrosion and some slip lines are visible in the fracture (SE image)

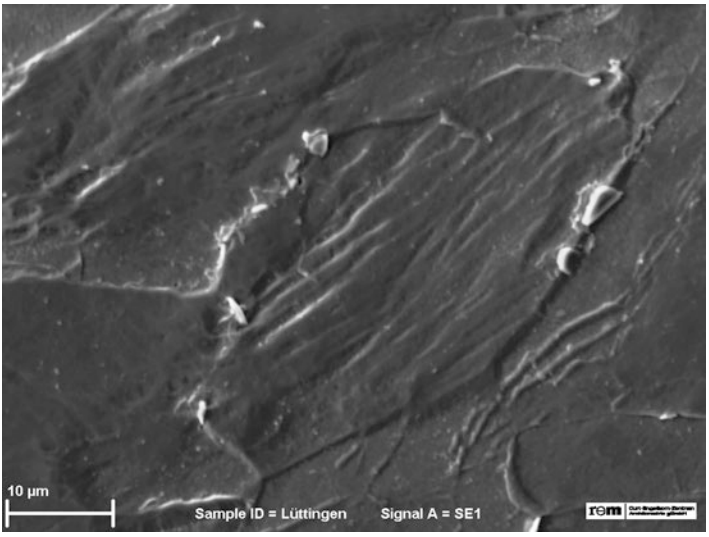

Fig. 3.22 Surface of a cold-worked iron chain link from a Roman mail shirt after etching with nital. Secondary electron image reveals spheroidal carbides at the grain boundaries

specific element. Notation K, L and M, which are used for X-ray emission lines, refer to the shell initially ionized, while Greek letters indicate the shell from which an electron originates to fill the vacancy, usually with a numerical subscript to denote the particular line of a series. Thus, when an electron is removed from the K orbital, being the innermost shell, and this electron vacancy is filled by an electron from an L level, the X-ray emission line is notated Kα, whereas if the electron is filled by an electron from an M level, the line is notated Kβ, or by filling other shells Lα, Lβ, Mα, etc., respectively (see Heinrich [25]; Reed [52]). The probability of the transition from L → K is always greater than that of the transition from M → K, but the binding energy increases from the outer to the inner shells as well as with increasing atomic number. Therefore the choice of accelerating voltage is depending on elements present within the target and must be balanced between the excitation energy needed and the background produced (see below). Measurement of the emitted X-ray signals can be performed by energy-dispersive (EDS) or wavelength-dispersive spectrometers (WDS), which instruments with the latter are traditionally called electron probe microanalysers (EPMA) with a much better spectral resolution and better detection limits, whereas energy-dispersive X-ray spectrometers (EDS or EDX) are commonly attached to conventional SEMs. It is possible to attach both EDS and WDS to a SEM, but the focusing geometry in an EPMA is designed for best angular and distance relationship between specimen, analysing crystals and detector to optimize analytical tasks, which is usually at the expense of the optical systems. A SEM is arranged for versatile applications and optimized to imaging methods.

Qualitative information can be obtained quickly by energy-dispersive X-ray spectrometry, but nevertheless quantitative chemical information is a basic task for electron microanalysis as it is generally to all X-ray spectrometry-based methods. Quantification can be achieved by different methods, but a correction of the matrix effects is essential, which is commonly applied in electron microanalysis by the so-called *ZAF* correction method (*Z* = atomic number differences influences the deceleration of electrons and background intensity; *A* = absorption of primary emitted characteristic X-rays; *F* = (secondary) X-ray fluorescence generated by characteristic and continuous X-rays). *ZAF* matrix correction procedures are nowadays software based, using tabulated values of constants. There are other approaches for correction procedures around, and again, standard literature should be consulted for basic knowledge and further reading (see Goldstein et al. [22]; Heinrich [25]; Reed [52]).

Standard-based methods are generally considered to be more accurate than so-called standard-less analysis but also more time-consuming, as sample and standard must be measured with the same parameters. Traditional standard reference methods usually calculate the concentrations *C* from the so-called *k* ratio of the matrix corrected intensities *I* of sample and standard after subtracting the background:

$$C_{\text{Sample}} = \frac{I_{\text{Sample}}}{I_{\text{Standard}}} \frac{(ZAF)}{(ZAF)}.$$

Standard-less methods have become more popular with computer-aided systems and high efficient silicon drift detectors (SDD), which are capable of processing high counting rates with comparatively high-energy resolution (≤121 eV for Mn-Kα are available at the moment). Most commercial EDX systems nowadays are installed with standard-less quantification software according to different mathematical and physical models, computer deconvolution of peak overlaps or stored standard references to compute concentrations. There is an ongoing progress in hardware and software technology to increase accuracy and precision of EDX analysis, and manufacturers have developed suitable user interfaces to make convenient handling available. The operators are therefore obliged to regularly control their results by measurements of appropriate standards under defined and reproducible conditions to ensure the accuracy of their analyses.

In contrast to most other analytical methods, the analytical data from X-ray microanalysis are highly space-resolved and provide direct information about compositional heterogeneity. Due to the finely focused electron beam and controlled scanning over the surface, the X-ray signals can be recorded in different ways. Micrometre-sized volumes of phases and particles can be analysed by point analysis, while line scans reveal the variation of selected elements along a line, which is, e.g. suitable to measure concentration gradients. A powerful application possibility is the two-dimensional mapping of X-ray intensities, which provides information on the spatial distribution of constituents within a selected area of interest (Fig. 3.23). After proper quantitative elemental map acquisition, modern EDX systems offer software tools that turn individual distributions of elements representing a chemically defined component of a complex multiphase material into a so-called phase image (Fig. 3.24), which is calculated by the spatial variability of specific X-ray intensity ranges at each pixel in the map (see Kotula et al. [31]).

Elastic scattering of the incident beam electrons is due to the retardation in the Coulomb field associated with atomic nuclei and implies almost no transfer of energy to the specimen electrons. When charged particles pass through the Coulomb field of a nucleus, they change direction, and the beam expands due to magnitude of

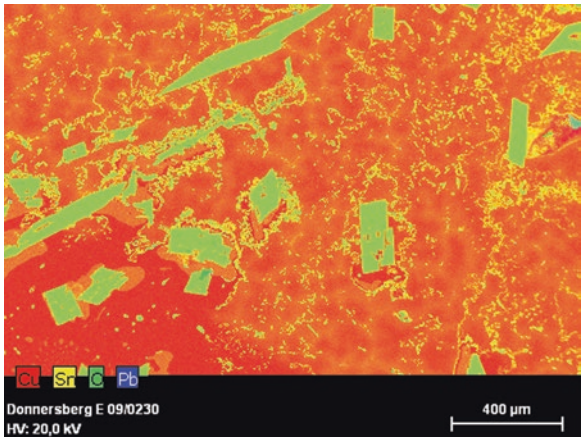

Fig. 3.23 Quantitative element map of a bronze casting waste from the oppidum on the Donnersberg in the Palatine Forest, Germany, showing the inhomogeneous distribution of tin and the presence of oxide phases

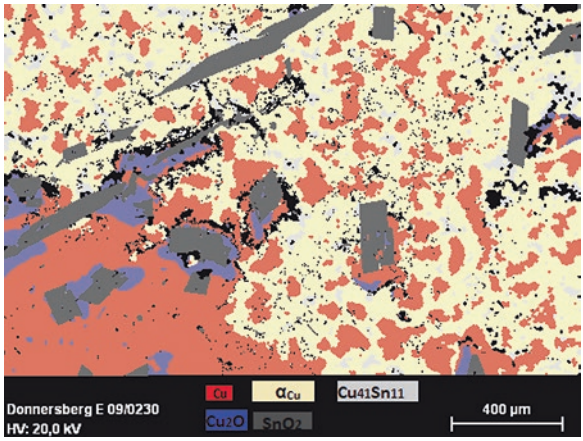

Fig. 3.24 Phase image created from quantitative element map (Fig. 3.23) showing selective internal oxidation of tin from a bronze alloy with precipitations of SnO_2 and formation of Cu_2O within the de-alloyed areas

the Coulomb force. Accumulated elastic scattering events that deviate the primary electrons' trajectory by an angle greater than 90° lead to an escape of so-called backscattered electrons (BSE) back out of the specimen's surface with nearly an equal energy (Heinrich [25], pp. 241–53). The deceleration of accelerated electrons and the amount of shift in direction depends on the Coulomb interaction between the positive field of the nucleus and the negative bound electrons. Coulomb force is proportional to atomic number of elements, for which reason the so-called backscattering coefficient, which is the ratio of backscattered to primary electrons incident normal to the flat surface, increases with increasing atomic number of the elements of the specimen.

Therefore, the image created by BSE signals is called compositional or atomic number contrast, which reflects differences in atomic number of elements or average atomic number for alloys and compounds (Fig. 3.25). BSE imaging is a very effective tool for metallography combined with X-ray microanalysis, but X-ray microanalysis should only be acquired together with a corresponding BSE image which shows a much better resolution than can be achieved by X-ray elemental map (see Goldstein et al. [22]). Indeed the backscattered electron image contains two types of information: compositional and topographic. In order to form an image with backscattered electrons, a semiconductor detector that has ring geometry is usually placed in their path above the sample to increase the angle of collection. The detectors have the capabilities of summing the segment's output signal eliminating topographic information and producing a pure compositional signal. Operating the BSE segments in pairs and then subtracting the segments' output signal yields topographic images (Fig. 3.26).

The backscattered signal in particular carries information about the crystal lattice and its orientation relative to the primary beam. Similar to optical isotropy and anisotropy, the proportion of backscattered electrons also depends on crystallographic isotropy or anisotropy which is associated with orientation and crystal properties. Lattice planes vertical to the surface allow electrons of a normal incident beam to penetrate more deeply into the lattice where they get absorbed, whereas

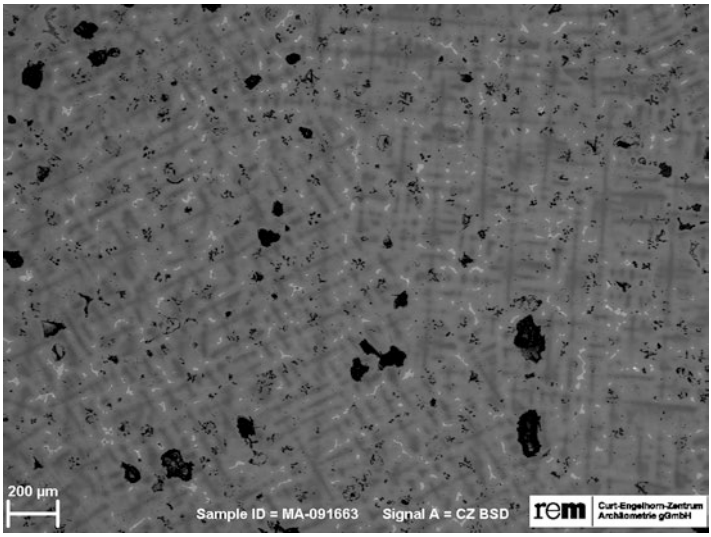

Fig. 3.25 Backscattered electron image of the bronze part of a bracelet from the Royal tomb of Lori Berd, Armenia. Compositional contrast reveals dendritic micro segregation (see Fig. 3.11). The α + δ shows the highest backscattering coefficient, whereas copper sulphides and pores are black

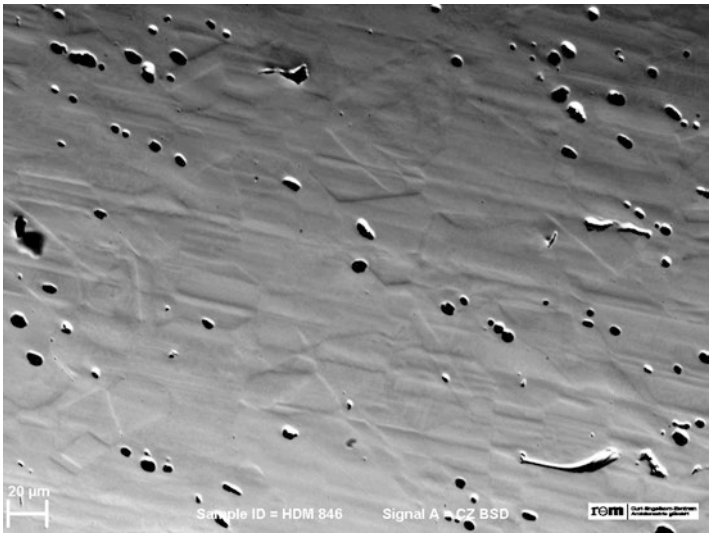

Fig. 3.26 Surface topography of the copper disc from Hornstaad with equiaxed twinned grains. The specimen is attack polished and imaged with two positively biased and two passive segments of the BSE detector

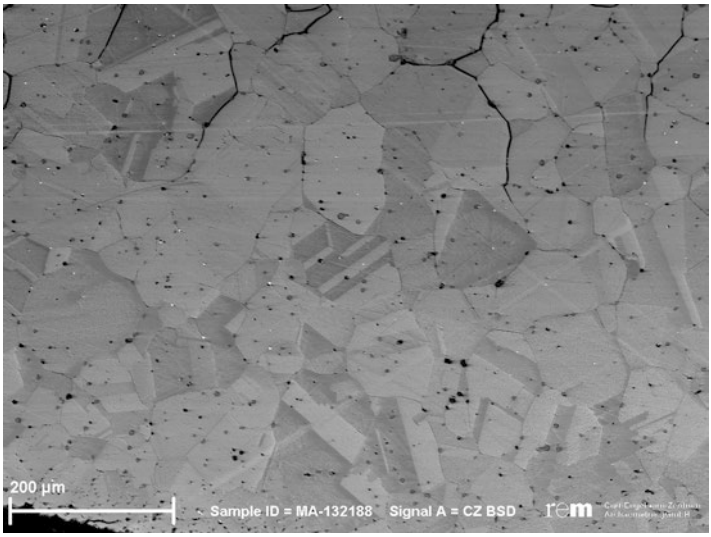

Fig. 3.27 Electron channelling contrast from a copper alloy belt sheet from Boğazköy, Turkey, showing grain boundaries and annealing twins. The specimen is attack polished, tilted and imaged with a positively biased BSE detector

planes parallel to the surface show a higher backscattering coefficient. The contrast resulting from crystallographic anisotropy is called orientation or channelling contrast. This contrast is usually weak, but by increasing the beam current and tilting the sample, grain boundaries, for example, can be visualized by BSE without etching, because of the different crystallographic orientation of the grains resulting in different grey levels shown in Fig. 3.27.

Channelling contrast by backscattered electrons is a subtle effect, and the evaluation of channelling patterns, which correspond to the lattice diffracting crystal planes, has been a useful application but on an academic level only. Crystallographic surface orientation evaluation by electron backscatter diffraction (EBSD) has become an additional and powerful standard characterization technique to scanning electron microscopy in metallography within the past two decades (see Rollett and Barmak [55]; Schwartz et al. [63]). The application of this technique to ancient metals has been very limited so far (e.g. Northover and Northover [40]). EBSD is performed by tilting the sample at a large angle of incidence of 70° to maximize the backscattering coefficient. Most systems use a forescatter geometry where diodes are mounted front of the sample near the phosphor screen to capture electrons with lower incidence scattered in a forward direction, called forescatter electrons (FSE). Fully automated commercial EBSD systems are readily available and can give extensive crystallographic orientation information of large areas in a sort time. EBSD is suitable for phase identification and for determination of orientation, size and shape of individual crystals quantitatively (see Schwartz et al. [63]).

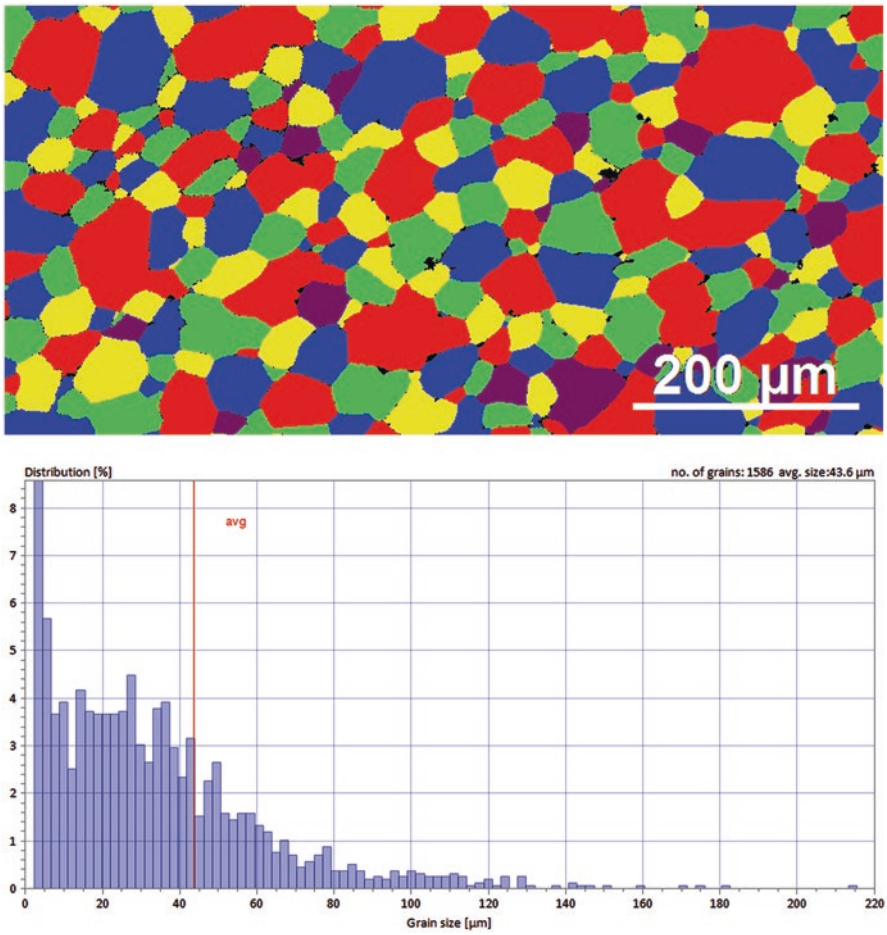

Fig. 3.28 EBSD grain size map with randomly coloured grains and grain size histogram of the recrystallized bronze alloy (11.7% Sn) of a belt plate from the Early Iron Age hoard from Fliess in Tyrol. (Image L. Palasse, Bruker Nano GmbH)

Figures 3.28 and 3.29 show EBSD pattern of a fully annealed Early Iron Age (HaC) bronze belt plate from the hoard of Fliess in Tyrol (Austria), with grain size distribution. It should be noted that grain size and orientation have been quantitatively acquired within one map in 20 min. EBSD pattern quality is extremely sensitive to surface disturbance, since the signals are generated from a layer about a few nanometres from the surface [55]. Any deformation or surface layer will disturb the diffraction bands and results in a loss of intensity and contrast, for which reason an accurate sample preparation is especially required, more so than for any other microscopical technique (see, e.g. Vander Voort [78, 79]; Witt and Nowell [83]).

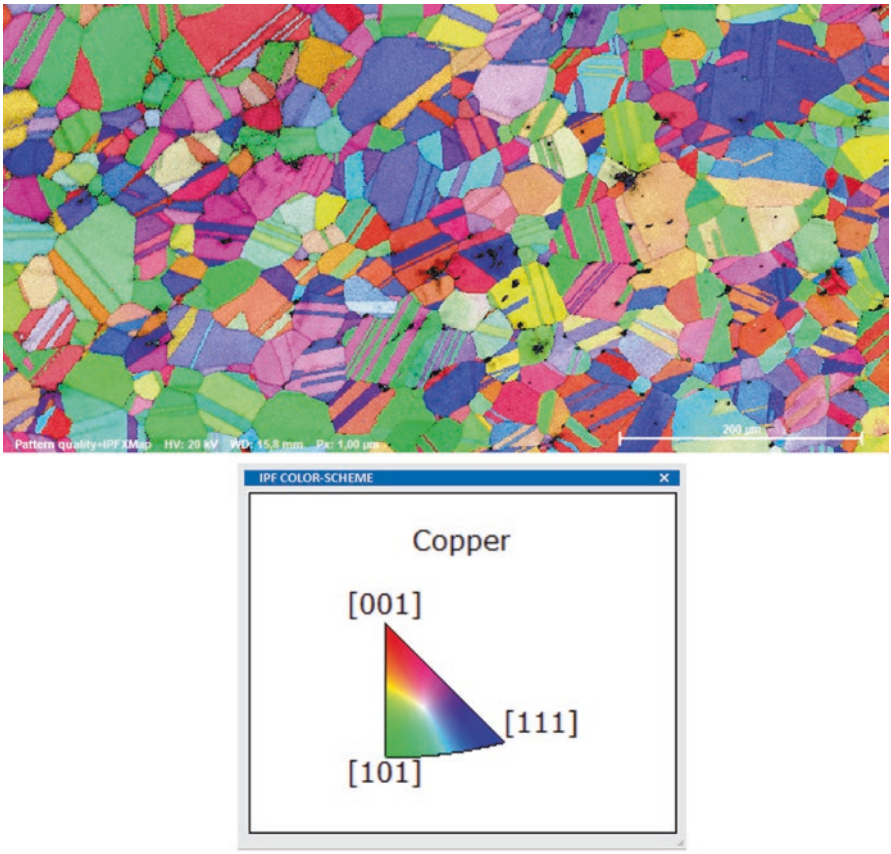

Fig. 3.29 RGB colour-coded EBSD orientation image with inverse pole figure (IPF) for the cubic class showing recrystallized α_{Cu}-solid solution grains with twins. Intermediate orientations are coloured by a mixture of the primary components red, green end blue. (Image L. Palasse, Bruker Nano GmbH)

The combined application of LOM and SEM is a powerful tool in the investigation of ancient metals, because the same specimen can be used without additional sampling.

For relocating regions of interest from light microscope to scanning electron microscopy, a significant microstructural feature is needed, which is not always the case, or hardness indentations can be used to mark the area of interest. For small samples from archaeological materials with some individualistic corrosion pattern, the relocation is usually not such a problem, but with increasing sample size, it can become quite time-consuming. Therefore, some microscope producers have developed a combined hardware and software solution, which is called correlative light electron microscopy (CLEM). It allows the flexible transfer of specimens from one microscope system to another without intermediate preparation steps.

3.3 Image Analysis and Quantitative Metallography

3.3.1 Image Analysis

After proper specimen preparation, the components of microstructure have to be revealed, identified, quantified and finally documented. Documenting important points in the microstructure at suitable magnifications is an essential task in the metallography of ancient metals. As mentioned before, sampling and analysing rare and valuable objects are very limited in scope, and the examination often cannot be repeated. Tiny and corroded samples are prone to be extruded by polishing and must be treated with care. Non-metallic inclusions or corrosion products that are present when the section is examined in the polished condition should be noted and evaluated before etching. Otherwise, they will either be dissolved or partially obliterated by etching. Especially the identification and quantification of non-metallic inclusions are tasks of increased significance for understanding ore sources, metallurgical processes and the history of implements (Sect. 4.4).

The early metallographers had to sketch their observations graphically by hand or make imprints directly from the etched surface, as Alois von Widmanstätten and others did with meteorites and wrought iron [69]. The adoption of photography to microscopic observation to document microstructure directly took place in the second half of the nineteenth century, which has been part of Henry Clifton Sorby's pioneering work [69]. Early metallographic microscopes had to use external cameras with additional oblique illumination, because of the low intensity of the illumination sources available [69]. Later microscopes had electric illuminations integrated and special attachments for a camera above the eyepiece. Professional metallographic microscopes, so-called metallographs, have been large instruments with integrated illumination source but with a separate attachment for the camera to permit permanent recording of the microstructure during microscopical observation [28, 58]. Today the illumination system is mounted beneath the specimen stage, and the camera is usually attached to the binocular head with a side port as a built-in integral part of the construction, connected directly to a display monitor of a computer with digital image software.

It is obvious that the documentation by photography is important in metallography to reproduce microstructural features observed and to make them comprehensible to others. Indeed, the earliest metallographic observations on prehistoric metals have still been recorded only through drawings (e.g. Rupe [56]); albeit further publications about metallographic studies of different ancient metal objects appeared, a few years later do already show micrographs on a respectable level [18, 19, 23, 24, 35].

Quantitative data of microstructures have been manually acquired by visual comparison, direct measurements at the microscope using inserted graticules in the ocular, or by grids applied to micrographs [14, 73, 75]. Scanning machines and television-equipped image analysers have been developed from the 1960s to 1980s [14, 17]. Nowadays, digital image acquisition has more or less totally replaced

analogue photographic techniques, and quantification is performed by computer-based digital image analysers [20, 57, 84]. As a basic principle, the digital image and the analogue photomicrograph are both two-dimensional reports from a two-dimensional view of a three-dimensional structure (see below). Indeed the major difference between digital and analogue imaging is that digital data are already stored as discrete picture elements (pixels) arranged in a regular two-dimensional grid. The digital image is therefore a function of two coordinates, meaning that each point P is at a specific location within a defined area A, each representing a different level of intensity. Therefore, all points or pixels forming an image with spatial arraignment of different intensities, grey levels or full colour, which characterize phases, interphases or pores, are captured. The fraction of all pixels with a specific intensity or colour represents the area fraction of each constituent of interest in the image. These defined positions of microstructural constituents render the image ready for automatic or semi-automatic measurements of size, geometry and fraction of microstructural constituents (see below).

3.3.2 Quantitative Metallography

Interpretation of microstructure under the microscope involves a high degree of empirical deduction. The identification of constituents is a common problem, but with skill and experience, it is possible to gain a detailed understanding. The application of electron microscope with its chemical and structural analysis ability has become a common tool in metallography, and it is suitable for identifying unknown phases by its variety of analytical techniques of characterization (Sect. 3.2). Finally, phase identification, indication of deformation, annealing or transformation processes and solidification structures still require a qualitative description of microstructure, though a micrograph is no description of condition of isolatable features but an experimental measurement of a system of interacting parts. Therefore, structure and mechanical properties of materials are strictly correlated. The determination of the relative quantity of constituents, whether it is a single-, two-phase or multiphase system; the presence and morphology of inclusions, pores and precipitations; or the relative specification of size of grains, such as descriptors of coarse or fine, would be another qualitative visual judgement. Indeed metallographers realized quite early that composition connects linearly with percentages of constituents and that there must be correlation of the microstructure with mechanical properties of materials [69, pp. 240–2].

Structurally, metals are made up of different phases, inclusions and pores, whose volume percentages, distribution, size, shape and orientation affect their properties. Therefore, the quantification of features visible in metallographic sections is essential for the understanding of relationships in microstructure. The quantitative characterization of this microstructural geometry is usually called stereology or quantitative metallography [14, 73].

It is beyond the scope of this chapter to cover the whole range of this topic, and standard monographs should be consulted whenever a quantitative evaluation is attempted (e.g. DeHoff and Rhines [14]; Exner and Hougardy [17]; Ohser and Mücklich [42]; Russ and DeHoff [57]; Underwood [73]). The application of stereological principles involves understanding the fundamental nature of microstructure and metallographic principles: firstly, traditional metallographic specimens are two-dimensional sections through three-dimensional solid bodies with spatial distributions and shapes of phases. From this two-dimensional view of a three-dimensional structure, planar data are obtained, which must be translated to spatial estimates of structure. To characterize microstructural features, a number of symbols and notations are advised by the International Society for Stereology ([20], tab. 17.1; [73], tab. 1.1; [75], tab. 6-1). Each notation is usually a combined term, which represents a geometrical element within a specific dimension. Conventionally, ratios are written as subscripts instead of fractions, in which the subscript indicates the unit of interest. So, for example, the notation N_A for number density is equivalent to $\frac{N}{A}$, which indicates the number N of a feature of interest per unit test area A [17, 73]. The basic notations and equations used throughout the book will be introduced in this chapter.

A planar section of a microstructure consists of areas, lines and points, which are in fact sections through particles, grains or interfaces, shown in Fig. 3.30. The area occupied by each constituent in a two-dimensional section is proportional to its three-dimensional volume, the line correspond to surface and point to a line in a solid body. Therefore, volume fraction V_v is considered to correspond to area fraction A_A or lineal fraction L_L or point count P_P (see below). Thus, the basic and simplest stereological equation is $V_v = A_A = L_L = P_P$ (e.g. Exner and Hougardy [17]). In practice are all microstructural components given in volume fractions, which are referred to as the unit volume of the microstructure. Therefore, the sum of the volume fractions

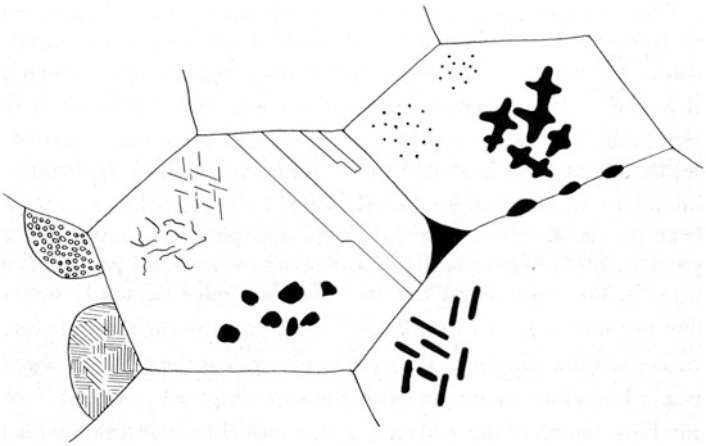

Fig. 3.30 Schematic illustration of a plane section through a polycrystalline body containing isolated microstructural features. (After Brandon [11])

of all phases in the test unit must be equal to one or, given in percentages, equal to 100%. Consequently, the volume fraction of a microstructural component must be in the range $0 \leq V_V \leq 1$ [21, p. 429]. Pores are by definition hollow, but in stereological practice, they are space filling volumetric elements like particles and must be treated as a microstructural component of equal value like a real spatial phase.

Furthermore, a metallographic section is a more or less arbitrary sectional view through the geometry of a particular microstructure. This implies that geometric shapes and quantities of constituents in the microstructure cannot be uniform or regular, and no constituents are exactly alike. Therefore, the problem of characterizing of a three-dimensional microstructure must rely on simplifying assumptions. Thus, any measurement of size, distribution or arrangement must be based on the general assumption that there is a certain probability of occurrence of events and that where the number of items is large, their distribution should be commonly described as Gaussian, even if the latter in many practical cases is not applicable. It becomes obvious that quantitative microstructure characterization can only be determined in statistical terms, so that the measurements must always be processed using an appropriate statistical procedure. Consequently, a metallographic specimen must be representative of the material, which is hundreds or thousands of times larger than the microstructure viewed under a microscope. Furthermore, the measured results should be comparable and the measurement reproducible. Representativeness and reproducibility are rarely given in studies concerning samples from objects of high cultural value. It is easy to understand that the application of stereological principles to archaeological and historical metals is limited and actually not regularly performed; nevertheless, it is useful to take the idea on-board and develop it for the future.

Before evaluating the practicality of quantitative methods to ancient metals, some general and historical aspects should be reviewed. According to Smith [69] scientists already realized the correlation between temperature and grain size in the eighteenth century by experiments and macroscopic observations of fractures. It is said that the first quantitative measurement using a microscope had already been performed by the French geologist A. Delesse, in 1848. Delesse demonstrated the proportional relation of area and volume in a random cross section [14, pp. 1–2]; 73, pp. 25–6], even though the relationship between grain size and mechanical properties, such as cold workability, had not been studied systematically by microscopy until the end of the nineteenth century [69, p. 241].

The relationship between heat treatment and microstructural geometry has been studied by measurements of lamellar spacing of pearlite or average grain intercept upon random sections [14]. Grain size estimation and the determination of volume fractions of particular constituents have been the oldest and are still the most common performed stereological measurements. To make a sound quantitative study of a metallographic specimen, several basic stereological measurement procedures and devices for quantitative analysis have been developed and improved, whereas many of these are now made obsolete by digital imaging technology. Nevertheless, it is useful to know the different methods, as some partly corroded samples do not allow standard quantitative digital image analysis, but for example, grain size or

volume fractions of specific microstructural constituents can be determined by manual measurements of microstructural images.

3.3.2.1 Methods of Measuring

3.3.2.1.1 Comparison Methods

Indeed, stereological measurements were laborious and time-consuming before the introduction of digital imaging technologies. Therefore, metallographers, especially in industrial quality control, wanted quick and easy methods for characterization of microstructures. Standard chart methods were introduced in the 1920s and were extensively used to estimate grain sizes, volume fractions and shapes of inclusions, pores or particles [75, p. 414]. Comparison charts are most simply used as wall charts or for direct comparison with the microscopical field in view, employing a recommended magnification, to select the most representative chart compared to the microstructure under investigation. Chart comparison ratings are generally semi-quantitative, subjective and not reproducible but sufficiently accurate for most commercial purposes. For research work, they should be replaced by stereological methods [17, pp. 83–87; 75, pp. 440–445, 502]. In spite of this, they are still in use, because they are fast and convenient to employ.

Grain sizes on worked objects can be measured using a grain size comparator eyepiece such as the graticule shown in Fig. 3.31 or compared standards given as wall charts. The most commonly used scale is that of the American Society for Testing of Materials (ASTM). By direct visual comparison at various magnifications, the ASTM number can be determined (see below). The ASTM has prepared a set of

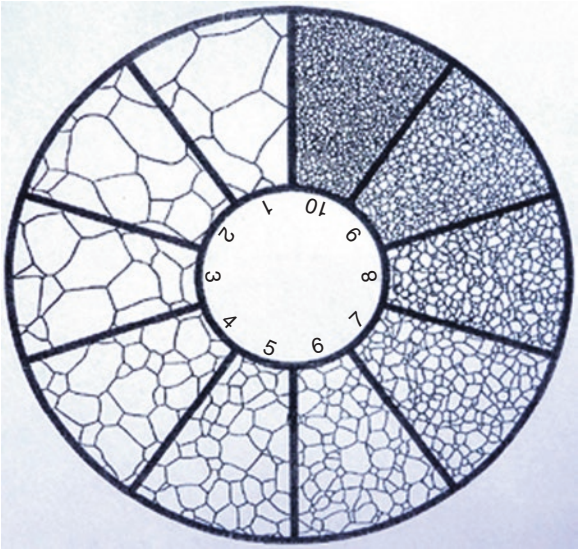

Fig. 3.31 Grain size eyepiece reticule for untwinned grains. For use with a 10x objective lens

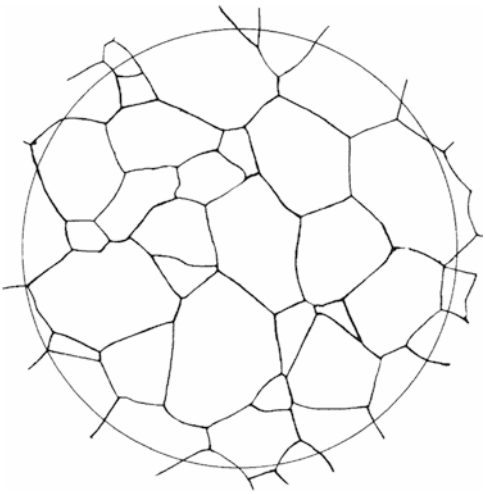

Fig. 3.32 ASTM grain size number 3 from Plate I for untwinned grains after flat etch at 100x magnification. (From ASTM E-112)

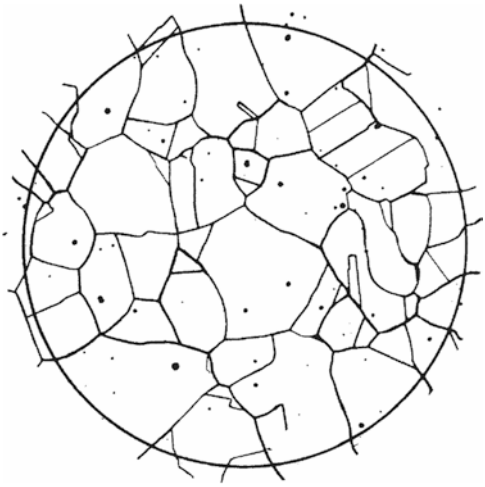

Fig. 3.33 ASTM grain size number 3 from Plate II for twinned grains after flat etch at 100x magnification. (From ASTM E-112)

standard charts for ferrous and non-ferrous materials, classified in four categories according to the appearance after etching and the absence or presence of twins, for which two examples are reproduced here in Figs. 3.32 and 3.33.

Great accuracy in this type of measurement is seldom required; what is useful is the approximation to an ASTM number that can readily be compared by another investigator. On the other side, it must be pointed out that great accuracy in this type of measurement cannot be achieved and bias will be introduced, which is usually 0.5–1 grain size number lower (ASTM E112-10). ASTM scale has been frequently used for the classification of grain sizes of archaeological iron objects (e.g. Piaskowski [47]; Pleiner [49]). The comparison chart method has also been the traditional approach for rating the inclusion content of steels. Vander Voort [74] has

given a detailed review about different charts and their application to the rating of non-metallic inclusions in modern steels. Comparison charts, such as the Swedish Jernkontoret or the German DIN 50602, have regularly been used to rate slag inclusions in archaeological wrought iron (e.g. Eichert et al. [15]; Hošek et al. [27]; Pleiner [49, 50]). Most of these charts were designed to categorize specific inclusions of steels, others to cover a wider range of ferrous alloys, but all of them have been developed using modern indirectly smelted iron, whose non-metallic inclusions originate from other metallurgical processes than ancient bloomery iron and do not adequately reflect the appearance of inclusions in ancient steels.

3.3.2.1.2 Feature Count

One basic stereological measurement is based on counting numbers N of individual features within a certain unit of interest, which can be a line L, an area A or a volume V, to obtain a representative average value. The number N of a specific microstructural constituent x is a fraction of the counted number of constituents of interest and the test unit. Therefore, N_L is the mean number per unit length (mm^{-1}), while N_A is the mean number per unit area (mm^{-2}) and N_V is the mean number per unit volume (mm^{-3}).

3.3.2.1.3 Point Counting

The point count method refers to the number of test points that fall in the unit of interest. The point fraction P_P is the ratio of the number of points in microstructural components of interest x to the total number of test points P_T in the test unit: $P_P = \frac{P_x}{P_T}$. This unit can be a certain test line, where the line intercept count P_L is the number of point intersections of this line (mm^{-1}), whereas P_A is the number of point intercepts in an area with regularly arrayed points (mm^{-2}). Again, this method is based on the general assumption that there is a certain probability that a randomly chosen point will include the microstructural component of interest. There can be confusion between number counting and point counting as they can be the same in certain cases, such as single-phase structures, so $P_L = N_L$. In a two-phase or multiphase microstructure, $P_L = 2\,N_L$.

3.3.2.1.4 Lineal Analysis

The lineal intercept method is employed randomly, or better using uniformly parallel arranged straight lines across the microstructure. The lineal fraction L_L is the ratio of the sum of individual lengths intercepted by microstructural constituent of interest L_X, divided by the total line length L_T: $L_L = \frac{\Sigma L_x}{L_T}$.

3.3.2.1.5 Areal Analysis

Area fraction A_A is the ratio of the sum of areas of microstructural constituent of interest A_x per total test unit area A_T: $A_A = L_L = \frac{\Sigma A}{A_T}$. Areal analysis is a planimetric method and can nowadays be performed with computer-aided digital image analysis. Before, manual area analysis must have been a troublesome undertaking, which involved the measurement with a planimeter, or cutting out the areas of interest from a photograph and comparing the weights of the pieces with the total weight of the photograph [73]. Area fraction has generally rarely been used, but Emmerling [16] applied this technique by cutting photographs to determining the volume fraction of pearlite and ferrite in prehistoric steel, which is now of historical interest.

The introduction of computer-based digital image analysis enabled high-speed (semi-) automatic image data acquisition. Automatic image processing techniques are usually based on image segmentation, which separates a digital image into sets of pixels sharing certain characteristics. These clusters of pixels should ideally correspond to a certain microstructural component, which can be characterized by contrast differences. For quantitative digital measurements, most basic stereological equations are still valid, but many classical stereological methods have become superfluous. Volume fraction V_v still equals area fraction A_A, which still equals point fraction P_P. The point fraction P_P would theoretically best denote the ratio of the pixel of interest to the total number of pixels of an image, but pixels are no points, which are dimensionless. Pixels have a finite area and are therefore generally thought to represent the smallest single components of a digital image. Therefore, area fraction A_A is now the quotient of N_p, the number of pixels of a determined phase and N_0 the total number of pixels in an image: $V_V = A_A = \frac{N_p}{N_0}$ [84].

3.3.2.2 Practical Application to Prehistoric and Historic Metals

Theoretically all stereological measurements can be used for ancient metals too, but quantitative characterization of microstructure is not often used for the metallographic investigation of ancient metals. Therefore, the real additional benefit of adopting every current practice in obtaining meaningful stereological data is not in sight at the moment, because of the lacking of statistical relevant data. Hence, we refer to the most regularly used measurements, their practical application and their values.

A general restriction to make a sound and representative quantitative study is often the small sample size or the condition. Surface corrosion and deep pitting corrosion sometimes do only allow the investigation of selected areas at high magnification, but increasing the magnification means reducing the observation area. Therefore, sizes and distribution of microstructural features are biased and require a higher number of areas observed to reduce the standard deviation, if possible.

A very important task for quantitative metallography is the quantification of volume fraction V_V of non-metallic inclusions (NMI) in modern as well as in ancient metals. Non-metallic inclusions are nearly always present in ancient metals, and in Sect. 4.3, the diversity and origin of them in the different alloys will be explained. Size, amount and composition of NMIs have a significant influence to mechanical properties of metals, but especially in ancient metals, they are a useful information source for metallurgical process applied (Sect. 4.3). The orientation of the plane-of-polish influences significantly inclusion rating, as orientation change, shape, number and distribution of the inclusions change [74, p. 13]. The amount of inclusions can be directly correlated to results of chemical analysis, as some elements have only very limited solid solubility, while others can partition between metallic and non-metallic phases (Chap. 5). Usually volume fraction V_V can immediately be measured from the image by area fraction A_A without great difficulty (Fig. 3.34).

If there are different inclusions within one sample, or the inclusions are multi-phased, it can be useful to define all phases as a single phase to get the total volume fraction of the inclusions and separate them in a second step. In the case of partly corroded microstructures, this method can be difficult or impossible, because of the possibly optical similarity of corrosion products and inclusions. For such samples, point or feature counting usually is the best and sometimes only solution, shown in Fig. 3.35.

One of the first things that we notice about ancient worked metals is how much the size of the individual grains vary, often even within the same object. Grain size has a significant effect to mechanical properties of alloys, such as hardness, yield strength or fatigue resistance, and most mechanical properties are improved as the size of the grains decrease. One of the functions of modern metallurgy is therefore

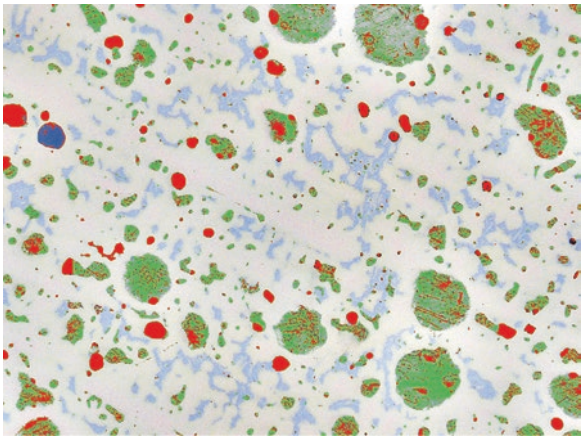

Fig. 3.34 Microstructure of a leaded high-tin bronze bracelet (28% Sn, 16.5% Pb) containing α + δ, lead globules, copper sulphide and copper oxide inclusions in α_{Cu} solid solution. Determination of V_V of non-metallic inclusions by digital area analysis is quick performed and oxide (not colour coded), and sulphide inclusions (red) can be separated. Lead content ($V_V = 11.9\%$) is underestimated, because of scratches and unsuccessful polishing

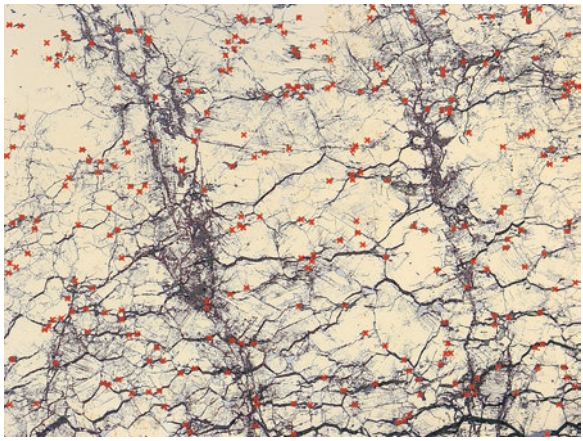

Fig. 3.35 Determination of V_V of non-metallic inclusions by feature count N_A within the corroded microstructure of a bronze belt from Denmark. The count of non-metallic inclusions is normalized by dividing by the area of the image. Volume fraction has been over estimated by digital area analysis A_A, because of the optical similarity of inclusions and corroded phases

to make the size of the metallic grains consistent across the alloy, depending on the engineering application that it is intended to be used for. Grain size measuring has thus to be adopted, and the most commonly used scale is the ASTM average grain size number *G,* whereas a wide variety of international standards exists. Grain size number represents the average planar grain size, and the relationship between ASTM grain size number and grain size depends on the measurement method, which are usually based on grain area or intercept length. Widely used is the planimetric method, known as the Jeffries method, which determines the grain size by calculating the number of grains *N* per unit area *A,* N_A. ASTM grain size number *G* is based on the formula: $N_{AE} = 2^{G-1}$, where N_{AE} represents the number of grains per square inch of at a magnification of 100x and N_A the number of grains per square millimetres by multiplying N_{AE} with 15.50 at a magnification of 1x (see ASTM E112-10; Geels [20]). Grain size measurement by the lineal intercept method has been developed by Emil Heyn, where grain boundary intersections *P* or the number *N* of intercepted grains are counted. The mean linear intercept length $\bar{L}$ is defined by $\bar{L} = \frac{1}{N_L} = \frac{1}{P_L}$ for space filling grains ($V_v = 1$), where *N* or *P* is divided by the total line length. The mean lineal intercept is related to ASTM grain size number *G* by the following empirical equation:

$$G = \left(-6.646 \log \bar{L}\right) - 3.298 \quad \left(\text{see Vander Voort}[75]\right).$$

With automatic or semi-automatic digital image analysis, grain size can be directly evaluated by measuring grain boundary lengths, shown in Fig. 3.36, which would be a fast and convenient method, but in practice lineal intercept methods are more suitable to non-uniform, intergranular corroded and twinned or slipped microstructures of ancient metals (Fig. 3.37).

For accuracy and precision, 50 grains in each of minimum three areas are required for modern alloys (ASTM E112-10), which is hard to realize for archaeological

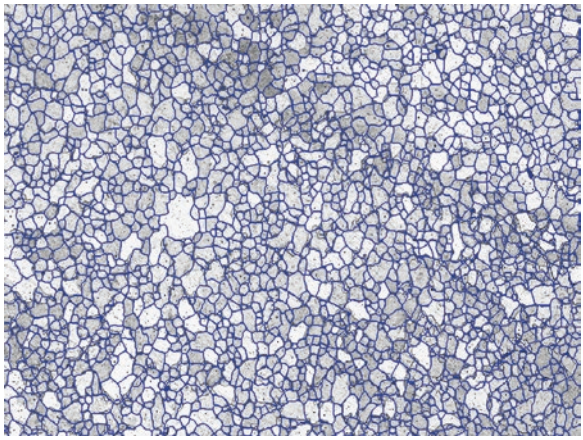

Fig. 3.36 Automatic measurement of grain boundaries of a ferritic mid-nineteenth century puddled iron from the fence of the church of Warburg-Dössel, Germany

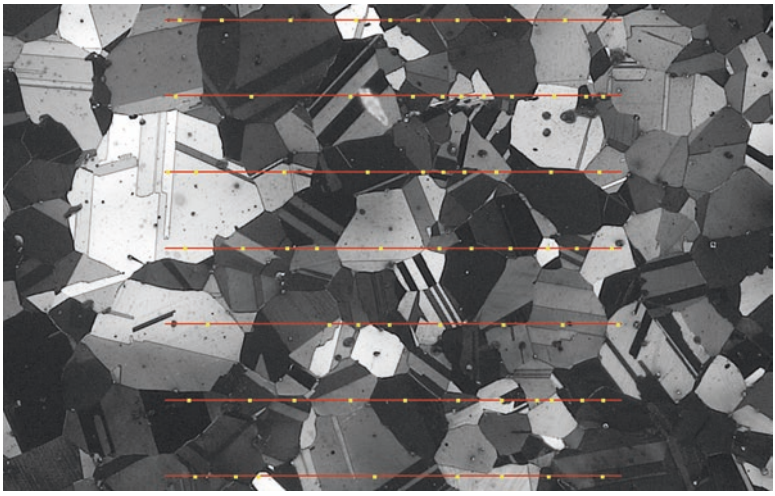

Fig. 3.37 Lineal intercept measurement $\bar{L} = \frac{1}{N_L}$ of grain diameters of a bronze belt from the hoard of Fliess, Austria, with twinned grains (see Fig. 3.29)

specimens. Figure 3.38 shows the typical mean grain sizes of ancient copper alloys, while Fig. 3.28 shows the grain size distribution within a single object.

When metals are as-cast and a dendritic structure remains, the mechanical properties of casting can be characterized by the distance between the dendrites, which is called dendrite arm spacing (DAS) or secondary dendrite arm spacing (SDAS). The DAS is best approximated by the dendrite cell intervals (centre-to-centre distance between two cells). The DAS can be measured by classical stereological

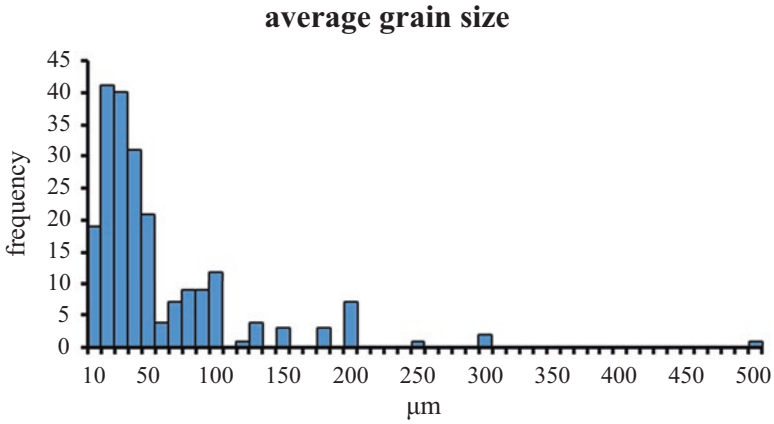

Fig. 3.38 Mean grain size distribution of ancient copper alloys (data taken from Northover [37–39] and own measurements)

intercept method, following this equation: $DAS = \frac{L}{n}$, where L is the length of the measured line and n number of arms intersected across a line traverse, or by areal analysis. Modern image analysing systems enable calibrated images so that the DAS can immediately be measured from the image. The DAS is the bigger, the slower the material solidifies (i.e. fewer but thicker dendrite arms at the same measuring length develop). Large, coarse dendrites generally mean that the cooling rate of the alloy in the mould was fairly slow, usually implying that heated or well-insulated moulds were employed. Finer dendrite arm spacing usually imply faster cooling rates.

3.3.3 Mechanical Properties

Actually, the testing of mechanical properties is no real development of modern material science. In modern material science, such tests are made to obtain information on elastic and plastic properties of an alloy, but the knowledge about plasticity of metals must have been already essential to prehistoric metalworkers. Literary evidence is given by Pliny (34, 94), who refers to malleable and castable bronze, which the latter would break by hammering or by the late medieval Islamic "Ayn-i-Akhbari" document, which reports the different qualities of brass (Sect. 5.1). Best archaeological evidence of mechanical testing of metals comes mainly from coins and of scrap metal depots. Coins with chisel cuts on the surface to expose forgeries are known from all periods [86, p. 237]. Such cutting or punching tests were not primarily focused to get information about the mechanical properties of the coins

but revealing their constitutions. Plated coins could have been easily detected by this ancestor of the modern notch impact test, and finally the revealed impact strength could also give information about the composition. Metallic deposits from Bronze Age to Roman times contain a variety of items crushed to pieces. Apart from ritual destruction or the antique practice for punishment "*damnatio memoriae*", the principal purpose for this destruction is a practical one, having the right size for melting down. Indeed some items show intensive bending and impacts from different tools. It seems as if the destruction should also reveal the mechanical properties such as hardness and tensile strength, to avoid the melting of unsuitable material. Like modern recycling, pre-industrial recovery of metals from scrap might have caused trouble without proper handling and separation.

3.3.3.1 Hardness Testing

Modern tensile testing is controlled tension until fracture, while hardness is a feature that is characterized by a measure of a metal's resistance to plastic deformation. The hardness test for bronze cannons developed in 1874 by Franz von Uchatius, an Austrian artillery general, for example, was nothing else than a falling chisel from a defined height of 25 cm [26, p. 2]. A related early approach to the problem was the scleroscope, which utilized graded steel balls that were dropped onto a metallic surface from a defined height (again 25 cm). Scleroscope hardness test is a dynamic measurement, at which the extent of rebound of the steel sphere was a measure of the hardness of the metal [26, pp. 76–78]. The main difference between modern mechanical testing of materials compared to empirical individual tests is to measure the behaviour of metals when subjected to certain reproducible conditions. Friedrich Mohs, a German mineralogist, developed one of the earliest reliable diagnostic hardness tests in 1812. The Mohs hardness test compares the resistance of a mineral to being scratched by ten reference minerals with different hardness. The Mohs scale is not suitable for metals, as it is strongly nonlinear and the hardness differentiation is too low. Scratching indeed had been adapted to metals but has been nearly totally replaced by methods in which indenters of different size and form are forced into the surface of a material by means of an applied load. Rockwell hardness testing machines use conical diamond or steel ball penetrators, equally to Brinell hardness testers, which also use a ball intender, while Knoop and Vickers hardness tests are performed by diamond pyramids. The test force (nowadays given in N or kgf) presses the intender into the surface of the specimen (in mm^2) for a specific loading time (in s), after which the intender is pulled back and the shape of intention can be measured: the smaller the indentation, the harder the material. Generally, the hardness values are based on applied test force F divided by the intended surface area A ($H = \frac{F}{A}$) and can be given in kilogrammes-force per square millimetre (Kgf/mm^2) or kilopond per square millimetre (Kp/mm^2). Hardness values can also be converted to SI units and given in Newton per square millimetre (N/mm^2) by multiplying with the standard gravity 9.80665 m/s^2. Indeed hardness is not a single fundamental

property, as the shape of the intenders influences the extend of elastic and plastic deformation of the surface, for which reason the general relationship of hardness values equates the test force per indentation size and must be calculated individually for each testing method by their specific equations (see Geels [20, pp. 626–39]; Vander Voort [75, pp. 339–66]). Therefore, hardness values are usually given without units in hardness numbers, using abbreviations for the method applied, the load used in kgf and ideally also the loading time (time is specified for modern hardness testing machines). So Knoop (HK) and Vickers hardness (HV), in the Anglo-Saxon language area also Diamond Pyramid Hardness (DPH) or Diamond Pyramid Number (DPN), are clearly characterized by this nomenclature, while Brinell hardness number (HB) must give the material of the ball intender, like HBS for steel or HBW for a tungsten carbide intender, just as Rockwell hardness (HR) must supply a scale symbol which gives form and force of the intender. For example, HRB would be a steel ball with 100 Kgf, while HRA and HRC would be a diamond cone (see Geels [20], tab. 21.2; Herrmann [26], pp. 29 tab. 1).

Hardness values achieved by different methods are not directly comparable but can be converted by the use of conversion charts (ASTM E140). These tables are based on empirical data, so that the accuracy of the conversion depends on the accuracy of the provided data and the resulting curve fits. For a quick comparison of hardness values, some simple hardness conversation equations are available giving approximate equivalents [20, p. 643].

All these conventional indentation hardness testing methods ignore the elastic deformation, and hardness is exclusively determined by the plastic indentation depth. To include the plastic as well as the elastic response of the tested material, Martens hardness testing (HM), formerly known as Universal hardness (HU), has been developed. Martens hardness uses mostly a Vickers indenter and is determined by instrumented measurement during application of a test force. Test force and the depth of indentation are recorded during the penetration, which makes it suitable for materials with low modulus of elasticity and composites [26, p. 186-; 61]. Martens hardness values are related to the sum of plastic and elastic indentation depths and are given in N/mm^2. Hardness values given in SI units but determined by conventional indentation hardness testing are not identical to Martens hardness values by the reason mentioned before.

3.3.3.2 Practical Application to Prehistoric and Historic Metals

Most modern mechanical test procedures like tensile test are not suitable for cultural objects, as it implies the total destruction of the sample, albeit it has been sporadically applied (e.g. Hadfield [23]; Salin and France-Lanord [58]; Zwicker [85]). Hardness testing is the only reasonable method combined with the metallography of ancient metals, as it leaves a small indentation and other mechanical properties may be estimated from hardness data. As tensile strength and hardness are both indicators of the resistance of a metal to plastic deformation, they correlate roughly linearly for several metals.

Dynamic measurements like those that scleroscopic hardness has only been sporadically applied to archaeological metals (e.g. Mathewson [35]), while static indentation tests are usual. The test forces for standard Rockwell method are very high (>10 Kgf) and therefore not suitable for testing ancient metals, because of the low sample sizes. Therefore, Rockwell hardness testing has hardly been performed but then converted to Brinell and Vickers hardness values (e.g. Anteins [2]; Arrhenius [3]). Brinell hardness test is the oldest of modern indentation tests and has been widely used in industry and research [75, p. 339], but it has been less applied to ancient metals (e.g. Hadfield [23]; Sperl [70]). In practice for small-sized samples, the microhardness tests with Knoop (e.g. Panseri and Leoni [44]) and most of all Vickers intenders have been proven successfully and are commonly used. The advantages of the microhardness tests are that only a very small sample of material is required and that it is valid for a wide range of test forces. Martens hardness (HM) testers are not yet widely distributed, and therefore the application to ancient metals is still quite rare (e.g. Schwab [62]). It should be noticed that some older publications also use the abbreviations MH, HM or Hm (e.g. Pleiner [49]; Thomsen [72]). These abbreviations only refers to hardness measurement with a microhardness tester after Hanemann, which is based on a Vickers diamond pyramid with small test loads where the area of the indentation may be directly measured instead of measuring the lengths of the diagonals.

The application of hardness testing to ancient metals offers valuable information about mechanical properties and completes characterization without great effort. The inhomogeneity in composition and the effects of plastic deformation, quenching or annealing can be illustrated by mapping hardness distributions in correspondence to overview images or drawings, as it is used for iron objects (e.g. Eichert et al. [15]; Pleiner [50]). The carbon contents of quench-hardened steels, for example, can be roughly estimated by microhardness testing without any need of chemical analysis. Precision and accuracy of hardness tests must be checked regularly by reference test blocks having different levels of hardness.

In a similar manner, quantitative methods can be applied to microstructural studies of prehistoric metals. It is reasonable to discuss the usefulness of bulk hardness or representativeness of mean values of microhardness. Measuring macrohardness with larger forces is usually not possible because of the mostly small sample size. So loads of 1 kgf or less must be used, which raise measurement errors, material influences and load dependence. At least five to ten hardness readings are required for a representative bulk hardness value of a relatively homogeneous material. For the determination of a significant mean hardness of inhomogeneous material, statistical methods are recommended.

The mean value of this heavily leaded alloy was determined 78 HV 0.1 ± 4 after 30 hardness indentations with 100 gf test force. The same result has been achieved after 20 hardness indentations, and after 10 indentations, the result diverts only 2% relative. Indeed a divergent hardness of 62 HV 1 ± 3 has been achieved after 20 hardness indentations with 1 kgf test force. This result has already achieved after 10 indentations. Between 10 and 20 microhardness, indentation seems to be enough for characterizing the mean hardness of leaded cast bronze, but the load dependence clearly becomes obvious. The microhardness with low test force represents the

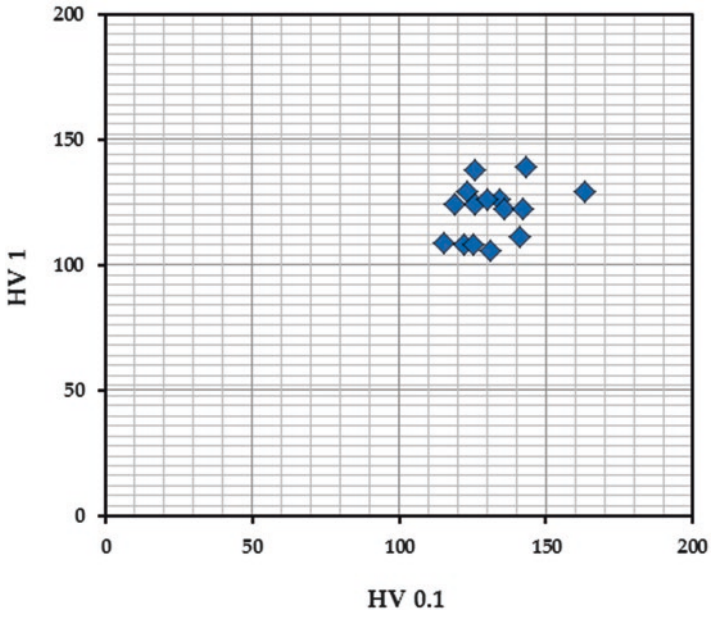

Fig. 3.39 Hardness distribution within one sample from a worked and partly annealed bronze situla from the Late Iron Age oppidum of Manching, Bavaria. Hardness testing has been performed at 0.1 kgf with a mean of 132 HV 0.1 and at 1 kgf with a mean of 121 HV 1, at which microhardness is biased by local inhomogeneity of microstructure

α_{Cu}-solid solution, whereas the hardness with heavier test forces is affected by the irregular distributed lead particles. Mean values of life-sized statues vary between 70 HV 0.1 and 120 HV 0.1, whereas typical mean values measured with higher test forces is 40–80 HV (see Leoni [33, p. 192]; Raub [51, p. 352]; Willer et al. [82], tab. 1).

Comparison between single-phased wrought copper and silver alloys have shown that there is usually not much deviation between mean values of different test force, but the precision of a lower test force is naturally more influenced by microstructural inhomogeneity (Fig. 3.39). The precision is usually between 10% and 20% relative for inhomogeneous worked and annealed objects, while the precision for mean hardness values of fully annealed objects is usually between 1% and 10% relative.

The hardness, obtained on a microscale using tiny indenters and microscopes to measure the size of the indentation, do not give large differences between the Brinell and Vickers numbers, but there are systematic variations in the two numbers that are addressed in the comparison charts shown in Fig. 3.40.

These charts will be useful in further comparison of data related to microhardness discussed later in the volume or given as data for individual alloying systems. Hardness is usually inversely proportional to brittleness. As alloys are cold-worked, dislocations pile up, and the ability of the alloy to be cold-worked further drops. The hardness increases until the alloy may become too brittle to actually be used in

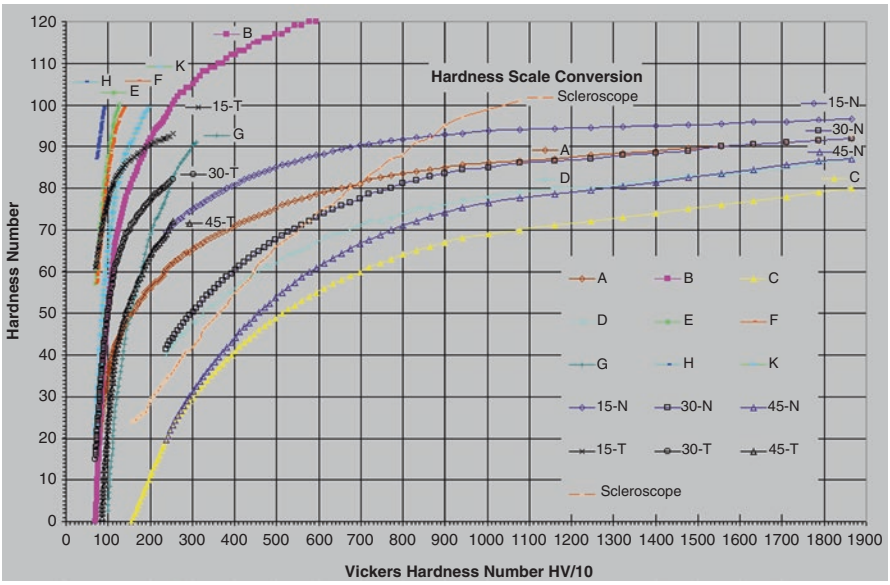

Fig. 3.40 Comparison of the Vickers hardness with 10 kgf compared with Hardness values in a number of different scales. For example, a Vickers hardness of 110 HV 10 gives a Brinell hardness of about 70 HB. From http://www.gordonengland.co.uk (2018)

practice without cracking. Annealing of the alloy will reform the grain structure and allow the dislocation density to be relieved. The effects of annealing in different alloy systems will be discussed later in relation to individual alloys.

References

1. Aliya, D.: Metallographic sectioning and specimen extraction. In: Vander Voort, G.F. (ed.) Metallography and Microstructure ASM handbook 9, pp. 229–241. ASM International, Materials Park (2004)
2. Anteins, A.K.: The structure and manufacturing techniques of pattern-welded objects found in the Baltic States. J. Iron Steel Inst. **206**, 563–571 (1968)
3. Arrhenius, B.: Technische Analysen der Schwerter von Elvran und Gravråk, Norwegen. In: Müller-Wille, M. (ed.) Zwei karolingische Schwerter aus Mittelnorwegen. Studien zur Sachsenforschung, vol. 3, pp. 155–167. Lax, Hildesheim (1982)
4. ASTM E112-10: Standard Test Methods for Determining Average Grain Size. ASTM International, West Conshohocken (2010)
5. Beraha, E.: New metallographic reagents for stainless steel and heat-resisting alloys. J. Iron Steel Inst. Jpn. **204**, 248–252 (1966)
6. Beraha, E.: Metallographic reagents based on Sulphide films. Pract. Metallogr. **7**(5), 242–248 (1970)
7. Beraha, E., Shpigler, B.: Color Metallography. American Society for Metals, Metals Park (1977)

8. Blet-Lemarquand, M., Da Mota, H., Gratuze, B., Leusch, V., Schwab, R.: Material sciences applied to West Hallstatt Gold. In: Schwab, R., Milcent, P.-Y., Armbruster, B., Pernicka, E. (eds.) Early Iron Age Gold in Celtic Europe. Forschungen zur Archäometrie und Altertumswissenschaft 6.1, pp. 101–132. Verlag Marie Leidorf GmbH, Rahden/Westf (2018)
9. Bousfield, B.: Surface Preparation and Microscopy of Materials. Wiley, Chichester (1992)
10. Bramfitt, B.L., Lawrence, S.J.: Field metallography techniques. In: Vander Voort, G.F. (ed.) ASM Handbook Volume 9: Metallography and microstructure, pp. 478–492. ASM International, Materials Park (2004)
11. Brandon, D.G.: Modern Techniques in Metallography. Butterworth, London (1966)
12. Bühler, H.-E., and Hougardy H.P.: Atlas of interference layer metallography. Deutsche Gesellschaft für Metallkunde, Oberursel (1980)
13. Darling, A.S., Healy, J.F.: Micro-probe analysis and the study of Greek gold-silver-copper alloys. Nature. **231**, 443–444 (1971)
14. DeHoff, R.T., Rhines, F.N. (eds.): Quantitative Microscopy. McGraw-Hill, New York (1968)
15. Eichert, S., Mehofer, M., Baier, R.: Archäologische und archäometallurgische Untersuchungen an einer karolingerzeitlichen Flügellanzenspitze aus dem Längsee in Kärnten/Österreich. Archäologisches Korrespondenzblatt. **41**, 139–154 (2011)
16. Emmerling, J.: Technologische Untersuchungen an eisernen Bodenfunden. Alt-Thüringen. **12**, 267–319 (1972)
17. Exner, H.E., Hougardy, H.P.: Quantitative Image Analysis of Microstructures: A Practical Guide to Techniques, Instrumentation and Assessment of Materials. DGM, Oberursel (1988)
18. Foote, H.W., Buell, W.H.: Composition, structure, and hardness of some Peruvian bronze axes. Am. J. Sci. **34**, 128–132 (1912)
19. Garland, H.: Metallographical researches on Egyptian metal antiquities. J. Inst. Met. **10**, 329–343 (1912)
20. Geels, K.: Metallographic and Materialographic Specimen Preparation, Light Microscopy, Image Analysis and Hardness Testing. ASTM International, West Conshohocken (2007)
21. Gokhale, A.M.: Quantitative Characterization and Representation of Global Micreostructural Geometry. In: Vander Voort, G.F. (ed.) Metallography and Microstructure ASM Handbook 9, pp. 428–447. ASM International, Materials Park (2004)
22. Goldstein, J.I., Newbury, D.E., Joy, D.C., Lyman, C.E., Echlin, P., Lifshin, E., Sawyer, L., Michael, J.R.: Scanning Electron Microscopy and X-Ray Microanalysis. Springer, New York (2003)
23. Hadfield, R.: Sinhalese Iron and steel of ancient origin. J. Iron Steel Inst. **85**, 134–186 (1912)
24. Hanemann, H.: Metallographische Untersuchung einiger altkeltischer und antiker Eisenfunde. Internationale Zeitschrift für Metallographie. **4**, 248–256 (1913)
25. Heinrich, K.F.J.: Electron Beam X-Ray Microanalysis. Van Nostrand Reinhold Company, New York (1981)
26. Herrmann, K. (ed.): Hardness Testing: Principles and Applications. ASM International, Materials Park (2011)
27. Hošek, J., Bárta, P., Šmerda, J.: Metallographic examination and reconstruction of the 6th century lombardic sword from Kyjov. Mater. Manuf. Process. **32**(7–8), 885–899 (2017)
28. Kehl, G.L.: The Principles of Metallographic Laboratory Practice. McGraw-Hill, New York/London (1939)
29. Klemm, H.: Farbenätzungen des Feingefüges der Metalle mit Natriumthiosulfat. Metallkundliche Berichte 45. Verlag Technik, Berlin (1952)
30. Klemm, H.: Anwendungsmöglichkeiten des Natriumthiosulfat-Verfahrens. Prakt. Metallogr. **5**, 163–167 (1968)
31. Kotula, P.G., Keenan, M.R., Michael, J.R.: Automated analysis of SEM X-ray spectral images: a powerful new microanalysis tool. Microsc. Microanal. **9**(1), 1–17 (2003)
32. Lang, J.: Iberian Falcata in the British museum. In: Pernicka, E., Schwab, R. (eds.) Under the volcano. Forschungen zur Archäometrie und Altertumswissenschaft 5, pp. 49–57. Marie Leidorf, Rahden/Westf (2014)

33. Leoni, M.: Metallographic investigation of the horses of san Marco. In: Perocco, G. (ed.) The Horses of San Marco. Venice, pp. 191–199. Olivetti, Milano (1979)
34. Lyman, T. (ed.): Metallography, Structures and Phase Diagrams ASM handbook 8. American Society for Metals, Metals Park (1973)
35. Mathewson, C.H.: A metallographic description of some ancient Peruvian bronzes from Machu Picchu. Am. J. Sci. **190**(240), 525–616 (1915)
36. Meeks, N., Cartwright, C., Meek, A., Mongiatti, A. (eds.): Historical Technology, Materials and Conservation: SEM and Microanalysis. Archetype, London (2012)
37. Northover, J.P.: Metal analysis and metallography of early metal objects. In: Vandkilde, H. (ed.) From Stone to Bronze. The Metalwork of the Late Neolithic and Earliest Bronze Age in Denmark, Jutland. Archaeological Society Publications 32, pp. 321–358. Jutland Archaeological Society, Aarhus (1996)
38. Northover, J.P.: Analysis of copper alloy metalwork from Arbedo TI. In: Schindler, M.P. (ed.) Der Depotfund von Arbedo TI und die Bronzedepotfunde des Alpenraums vom 6. bis zum Beginn des 4. Jh. v.Chr.. Antiqua 30, pp. 289–315. Schweizerische Ges. für Ur-und Frügeschichte, Basel (1998)
39. Northover, J.P.: Analysis and metallography of copper alloy metalwork. In: Lippert, A., Stadler, P. (eds.) Das spätbronze- und früheisenzeitliche Gräberfeld von Bischofshofen-Pestfriedhof. Universitätsforschungen zur prähistorischen Archäologie 168, pp. 351–384. R. Habelt, Bonn (2009)
40. Northover, S., Northover, P.: Applications of electron backscatter diffraction in archaeology. In: Meeks, N., Cartwright, C., Meek, A., Mongiatti, A. (eds.) Historical Technology, Materials and Conservation: SEM and Microanalysis, pp. 76–85. Archetype, London (2012)
41. Ogilvie, R.E.: Electron microanalysis of paint samples from the Bersheh sarco-phagus. In: Application of Science in the Examination of Works of Art, pp. 223–228. Museum of Fine Arts, Boston (1965)
42. Ohser, J., Mücklich, F.: Statistical Analysis of Microstructures in Materials Science Statistics in Practice. Wiley, Chichester (2000)
43. Olsen, S.L. (ed.): Scanning Electron Microscopy in Archaeology. BAR international series 452. BAR, Oxford (1988)
44. Panseri, C., Leoni, M.: Research on an Iron spearhead from the Etruscan sanctuary of Fanum Voltumnae, fourth to third centuries B.C. In: Levey, M. (ed.) Archaeological Chemistry. A Symposium, pp. 205–229, Philadelphia (1967)
45. Perryman, E.C.W.: The examination of metal surfaces. In: GKT, Conn., Bradshaw, F.J. (eds.) Polarized Light in Metallography, pp. 70–87. Butterworths Scientific Publications, London (1952)
46. Petzow, G.: Metallographic Etching: Techniques for Metallography, Ceramography, Plastography. ASM International, Materials Park (1999)
47. Piaskowski, J.: Metallographic investigations of ancient Iron objects from the territory between the Oder and the basin of the Vistula River. J. Iron Steel Inst. **198**, 263–282 (1961)
48. Piccardo, P., Mille, B., Robbiola, L.: Tin and copper oxides in corroded archaeological bronzes. In: Dillmann, P., Beranger, G., Piccardo, P., Matthiesen, H. (eds.) Corrosion of Metallic Heritage Artefacts. Investigation, Conservation and Prediction for Long-Term Behaviour. European Federation of Corrosion Publications 48, pp. 239–262. Woodhead Publishing, Cambridge (2007)
49. Pleiner, R.: Die Technologie des Schmiedes in der Großmährischen Kultur. Slovenská Archeológia. **15**(1), 77–188 (1967)
50. Pleiner, R.: Zur Schmiedetechnik im römerzeitlichen Bayern. Bayerische Vorgeschichtsblätter. **35**, 113–140 (1970)
51. Raub, C.J.: Was kann der Archäologe von der Metallkunde erwarten? Fundberichte aus Baden-Württemberg. **10**, 345–365 (1985)
52. Reed, S.J.B.: Electron Microprobe Analysis, 2nd edn. Cambridge University Press, Cambridge (1993)

53. Reimer, L.: Scanning Electron Microscopy: Physics of Image Formation and Microanalysis. Springer series in optical sciences 45, 2nd edn. Springer, Berlin/Heidelberg (1998)
54. Roberts, G.: X-ray microanalyser. Archaeometry. **3**(1), 36–37 (1960)
55. Rollett, A.D., Barmak, K.: Orientation mapping. In: Laughlin, D.E., Hono, K. (eds.) Physical Metallurgy II, 5th edn, pp. 1113–1140. Elsevier, Amsterdam (2014)
56. Rupe, H.: Notitz über die chemische Untersuchung prähistorischer Gräberfunde von Castraneda. Verhandlungen der Naturforschenden Gesellschaft in Basel. **18**(1), 1–13 (1905)
57. Russ, J.C., DeHoff, R.T.: Practical Stereology, 2nd edn. Kluwer Academic, New York (2000)
58. Salin, É., France-Lanord, A.: Le fer à l'époque mérovingienne. Geuthner, Paris (1943)
59. Samuels, L.E.: Metallographic Polishing by Mechanical Methods, 3rd edn. ASM International, Materials Park (1982)
60. Schaaber, O.: Beiträge zur Frage des Norischen Eisens. Metallkundliche Grundlagen und Untersuchungen an Funden vom Magdalensberg. Carinthia I. **153**, 129–279 (1963)
61. Schadewald, I., Heermant, C., Dengel, D.: Martenshärteprüfung. Härterei-technische Mitteilungen. **56**(4), 236–241 (2000)
62. Schwab, R.: Evidence for carburized steel and quench-hardening in the 'Celtic' oppidum of Manching. Hist. Metall. **36**(1), 6–16 (2002)
63. Schwartz, A.J., Kumar, M., Adams, B.L., Field, D.P.: Electron Backscatter Diffraction in Materials Science, 2nd edn. Springer, New York (2009)
64. Scott, D.A.: Pre-Hispanic Colombian metallurgy: studies of some gold and platinum alloys. Ph.D. diss. University of London, London (1982)
65. Scott, D.A.: The metallographic preparation of ancient lead. Stud Conserv. **41**, 60–62 (1996)
66. Scott, D. A.: Copper and Bronze in Art: Corrosion, Colorants, Conservation. J. Paul Getty Press, Los Angeles (2002)
67. Scott, D.A.: Laboratory notes homemade equipment aids for metallographic sample preparation. The Conservator. **31**, 87–91 (2008)
68. Scott, D.A.: Colour metallography in the examination of ancient metals. Stud. Conserv. **59**, 113–122 (2014)
69. Smith, C.S.: A History of Metallography. The University of Chicago Press, Chicago (1960)
70. Sperl, G.: Zur Urgeschichte des Bleis. Z Met. **81**(11), 799–801 (1990)
71. Stokes, D.J.: Principles and Practice of Variable Pressure/Environmental Scanning Electron Microscopy (VP-ESEM). Wiley, Chichester (2008)
72. Thomsen, R.: Metallographic studies of an axe from the migration age. J. Iron Steel Inst. **204**, 905–909 (1966)
73. Underwood, E.E.: Quantitative Stereology. Addison-Wesley, Reading (1970)
74. Vander Voort, G.F.: Inclusion measurement. In: JL, McCall., French, P.M. (eds.) Metallography as a Quality Control Tool, pp. 1–88. Plenum Press, New York/London (1980)
75. Vander Voort, G.F.: Metallography, Principles and Practice. McGraw-Hill, New York (1984)
76. Vander Voort, G.F. (ed.): Metallography and Microstructure ASM handbook 9. ASM International, Materials Park (2004a)
77. Vander Voort, G.F.: Color metallography. In: Vander Voort, G.F. (ed.) Metallography and Microstructure ASM handbook 9, pp. 493–512. ASM International, Materials Park (2004b)
78. Vander Voort, G.F.: Metallographic specimen preparation for Electron backscattered diffraction part I. Pract. Metallogr. **48**(9), 454–473 (2011a)
79. Vander Voort, G.F.: Metallographic specimen preparation for electron backscattered diffraction part II. Pract. Metallogr. **48**(10), 527–543 (2011b)
80. Vilella, J.R., Kindle, W.F.: Sodium Bisulphite as an etchant for steel. Metal Progress. **76**(6), 99–100 (1959)
81. von Schwarz, M., Die Anwendung des Polarisationsmikroskopes bei der Untersuchung von Kupferlegierungen. Z. Met. **24**(5), 97–103 (1932)
82. Willer, F., Schwab, R., Mirschenz, M.: Römische Bronzestatuen am Limes: Archäometrische Untersuchungen zur Herstellungstechnik. Bonner Jahrbücher. **216**, 57–208 (2017)
83. Witt, R., Nowell, M.: Specimen preparation of difficult materials for EBSD characterization. Microsc. Microanal. **17**(S2), 414–415 (2011)

84. Wojnar, L., Kurzdłowski, K.J., Szala, J.: Quantitative image analysis. In: Vander Voort, G.F. (ed.) Metallography and Microstructure ASM handbook 9, pp. 403–427. ASM International, Materials Park (2004)
85. Zwicker, U.: Untersuchungen an einem Eisenbarren aus dem Depotfund von Renningen (Kr. Leonberg). Fundberichte aus Schwaben. **18**(1), 282–283 (1967)
86. Zwicker, U., Oddy, A., La Niece, S.: Roman techniques of manufacturing silver-plated coins. In: La Niece, S., Craddock, P. (eds.) Metal Plating and Patination, pp. 223–246. Elsevier, London (1993)